Chair of Drilling and Completion Engineering

Master's Thesis

Real Time In-Situ Monitoring of Cement Carbonation with Acoustic System

Sven Curis

November 2021

To my lovely parents and family

Affidavit

I declare in lieu of oath that I wrote this thesis and performed the associated research myself using only literature cited in this volume.

Eidesstattliche Erklärung

Ich erkläre an Eides statt, dass ich diese Arbeit selbständig verfasst, andere als die angegebenen Quellen und Hilfsmittel nicht benutzt und mich auch sonst keiner unerlaubten Hilfsmittel bedient habe.

Sven Curiš

Sven Curis, 30 November 2021

Abstract

In this thesis, the overview of the potential of carbon capture and storage projects is presented. As carbon dioxide is one of the main contributors to total greenhouse gas emissions, this could be a way to mitigate global greenhouse gas emissions in the future. The main problem of carbon dioxide injection is the carbonation process, which causes the increase of cement's permeability and reduction of its compressive strength. This could ultimately lead to the loss of well integrity. One of the methods which could monitor the carbonation in real-time is the acoustic method. The sonic velocity of ultrasonic waves which go through a certain cement density is in correlation with its compressive strength. This is of a great importance as the compressive strength of the cement may be monitored with the acoustic method. This method is already widely applicable as the Ultrasonic Pulse Velocity method to determine the quality of the concrete. Together with the correlation, the crack investigation also took place to determine the depth of cracks and correlate them with sonic velocity. Finally, the overall experimental procedure with the necessary apparatus is presented in this thesis along with the results and steps which were so far made.

Zusammenfassung

In dieser Arbeit wird ein Überblick über das Potenzial von Projekten zur Kohlenstoffabscheidung und speicherung gegeben. Da Kohlendioxid einer der Hauptverursacher der gesamten Treibhausgasemissionen ist, könnte dies eine Möglichkeit sein, die globalen Treibhausgasemissionen in Zukunft zu verringern. Das Hauptproblem bei der Injektion von Kohlendioxid ist der Karbonatisierungsprozess, der zu einer Erhöhung der Durchlässigkeit des Zements und einer Verringerung seiner Druckfestigkeit führt. Dies könnte letztlich zum Verlust der Integrität des Bohrlochs führen. Eine der Methoden, mit der die Karbonatisierung in Echtzeit überwacht werden kann, ist die akustische Methode. Die Schallgeschwindigkeit der Ultraschallwellen, die eine bestimmte Zementdichte durchdringen, steht im Zusammenhang mit seiner Druckfestigkeit. Dies ist von großer Bedeutung, da die Druckfestigkeit des Zements mit der akustischen Methode überwacht werden kann. Diese Methode ist als Ultrasonic Pulse Velocity-Methode bereits weit verbreitet, um die Qualität des Betons zu bestimmen. Zusammen mit der Korrelation fand auch die Rissuntersuchung statt, um die Tiefe der Risse zu bestimmen und sie mit der Schallgeschwindigkeit zu korrelieren. Abschließend wird in dieser Arbeit der gesamte Versuchsablauf mit der notwendigen Apparatur vorgestellt, sowie die Ergebnisse und Schritte, die bisher gemacht wurden.

Acknowledgements

First of all, I am very grateful to my advisors from the Mining University of Leoben, prof. Kris Ravi and prof Michael Prohaska-Marchried for their guidance and giving me the opportunity to work in this project as the student assistant. Also, I would like to thank to my advisor from Gubkin University prof. Leonid Nikolaevich Litvinov, together with prof. Mikhail Gelfgat for accepting this idea and support when it was needed. Deep gratitude goes also to Alexander Fine for giving me technical advice about the project and always being there to help in the laboratory whenever was necessary.

I would also like to express my deep gratitude to my co-worker and friend Karez Abdulhameed. She was the person who introduced me this project and gave me always encouragement to push forward whenever I felt bad about something.

Last, but not least, all this would not be possible without the endless support of my parents and other family members, who supported me throughout the whole study program of Joint International Master Program in Petroleum Engineering. When I presented the idea to study in this program, they were all for it and supported me throughout the whole studies.

Sven Curiš

Contents

Chapter 1 Introduction

The Earth's climate is a complex system which includes multiple components of the whole planet. This system is confusing to understand since plenty of parameters influence it. Scientists have learned to understand this system, and therefore the leading conclusion is that people are causing an effect of global warming with which they influence the global climate in a negative way. Greenhouse gases are the number one reason for the global climate change. They are comprised of the following gases (Mathez, Smerdon, 2018):

- Carbon dioxide (CO_2),
- Methane (CH_4),
- Nitrous oxide (N_2O),
- Ozone (O_3) and,
- Water vapor (H_2O).

Carbon dioxide goes into the atmosphere in various ways, such as burning fossil fuels and as a product of chemical reactions. As a part of the biological cycle, carbon dioxide is absorbed by the trees, which causes emission reduction. Methane is emitted during the production and transport of coal, natural gas, and oil. Methane emissions also result from livestock and other agricultural practices, land use and by the decay of organic waste in municipal solid waste landfills. Nitrous oxide emits into the atmosphere in numerous ways, like from agriculture, industry and as a product of wastewater treatment (EPA, 2021).

As carbon dioxide has the greatest influence on climate change, handling and mitigating its emission has the greatest priority. Because it accounts for the majority of greenhouse gas emissions, its mitigation will have the greatest positive impact on the mitigation of climate change. Figure 1 shows the greenhouse gas emissions by gas based on 2010 data. (IPCC, 2014)

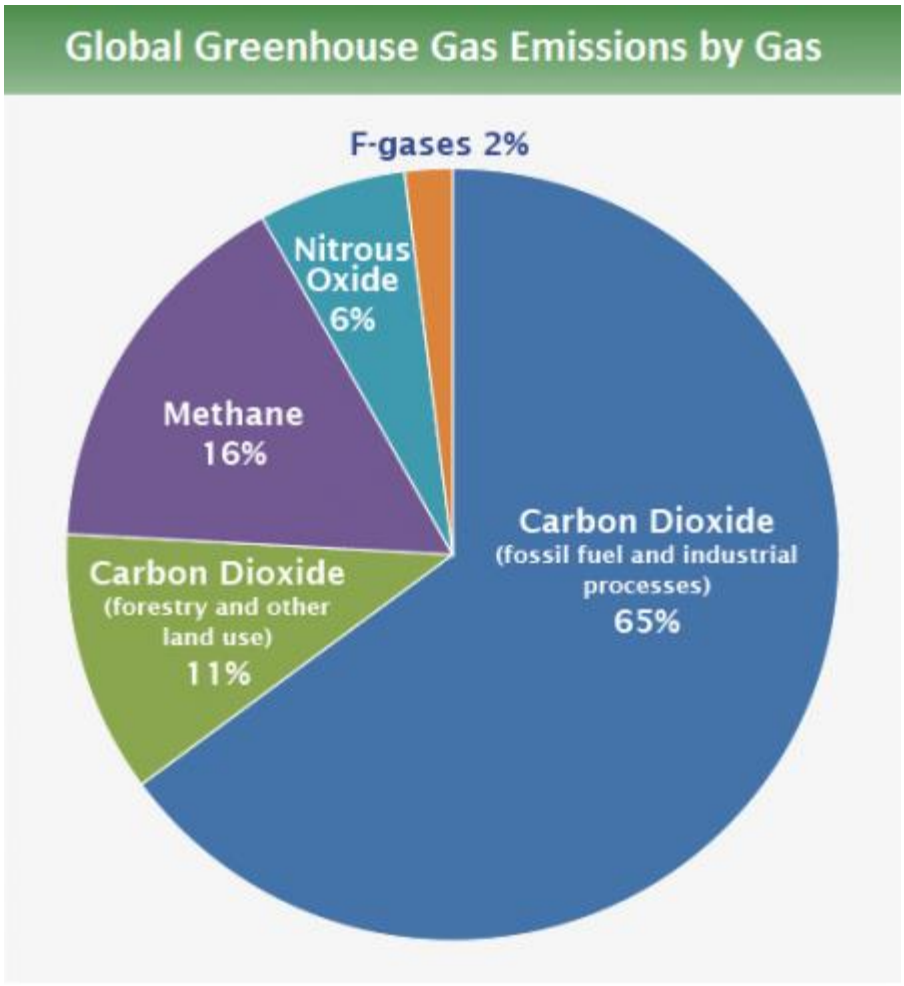

Figure 1: Global greenhouse gas emissions by gas (IPCC, 2014)

There are two methods in the oil and gas industry, which could contribute to global mitigation of carbon dioxide emissions. These are the carbon capture and storage (CCS) processes and the usage of carbon dioxide as an enhanced oil or enhanced gas recovery method. For these processes, capture systems will capture carbon dioxide, either from industrial facilities or from the atmosphere. Currently, capturing carbon dioxide typically takes place near to the storage reservoir, to avoid transport. Carbon dioxide is brought to the well site by pipelines from the capture locations. Depleted oil and gas reservoirs and depleted saline formations. For enhanced oil recovery, the selection of potential candidates is different. A necessary requirement is the presence of an intact cap rock, which forms a trap and traps the carbon dioxide in the reservoir. Based on geological factors, carbon dioxide turns to the supercritical state at the depths of 800 to 1000 meters. In this supercritical state, carbon dioxide uses all potential underground storage space. (Metz, 2005)

Cement is the main problem for carbon capture and storage projects. When cement is exposed to carbon dioxide, calcium bearing phases of the cement react with carbon dioxide, forming calcium carbonate and even more harmful bicarbonate. These reactions require a certain amount of water, for example as a free water from cement. The gaseous

carbon dioxide then dissolves in the water and penetrates the cement pores much quicker. The carbonation of oil and gas wells could lead to disastrous consequences.

Cement in oil and gas wells is an essential component to ensure the integrity of a well. After the casing string is run in an oil and gas well, cement is pumped into the well annulus between the casing and formation, which ensures that the casing is secured in place, and more importantly, that there are no migration paths for the formation fluids behind the casing. If these fluids are allowed to migrate behind the casing, the well integrity is compromised, and interventions are needed to take place in order to bring back full integrity of the well.

In order to gain a better understanding of the carbonation process and its influence on cement properties, this thesis proposes an analysis method in real-time and it could be performed under reservoir conditions. Design and construction of an autoclave, capable of carrying out such tests, and to monitor carbonation in real-time with the acoustic system, is the purpose of this thesis. To get a high reproducibility, a standardized experimental procedure is created.

Chapter 2 Carbon Dioxide Storage and Issues

In this chapter, the potential of mitigating carbon dioxide emissions within the oil and gas industry through the storage process is going to be discussed. There are two storage methods within the industry, namely:

- Carbon capture and storage and,
- Injection of carbon dioxide in enhanced oil or gas recovery projects.

As mentioned before, the greatest problem of carbon dioxide storage is the carbonation of cement, which gives us the products of calcium carbonate and bicarbonate. As this causes an increase of cement permeability and a decrease of compressive strength, it can cause a loss in well integrity. The full process of carbonation is also going to be discussed in this chapter.

2.1 Geological Carbon Dioxide Deposition

There are two different approaches for the geological deposition of carbon dioxide. One of the methods is the utilization of carbon dioxide as an enhanced oil or gas recovery method in active oil and gas fields. The other method is the permanent storage of carbon dioxide in (Metz, 2005):

- Depleted oil and gas reservoirs,
- Coal beds which are not minable and,
- Deep salt formations.

From the economic aspect, these approaches offer totally different opportunities. While the utilization of carbon dioxide already showed to be economically feasible, the storage of carbon dioxide could become economically feasible in the future. Figure 2 shows a map of the globe with indicators in locations of large scale carbon dioxide projects, which are either underway or proposed. (Metz, 2005)

Figure 2: Global locations of CCS projects (Metz, 2005)

Before the storage, carbon dioxide capture occurs. The carbon dioxide capture typically takes place at sizeable industrial plants, so-called point sources. Although capturing carbon dioxide out of the atmosphere is possible, it's not yet a viable option. There are three carbon capture systems, namely (Metz, 2005):

- Post-combustion,
- Oxy-fuel combustion and,
- Pre-combustion capture.

Figure 3 shows the elemental processes of those three systems. Sometimes carbon dioxide capture occurs directly from industrial process streams, where natural gas purification could be given as an example. Other examples are the production of synthetic gas, cement, or steel. (Metz, 2005)

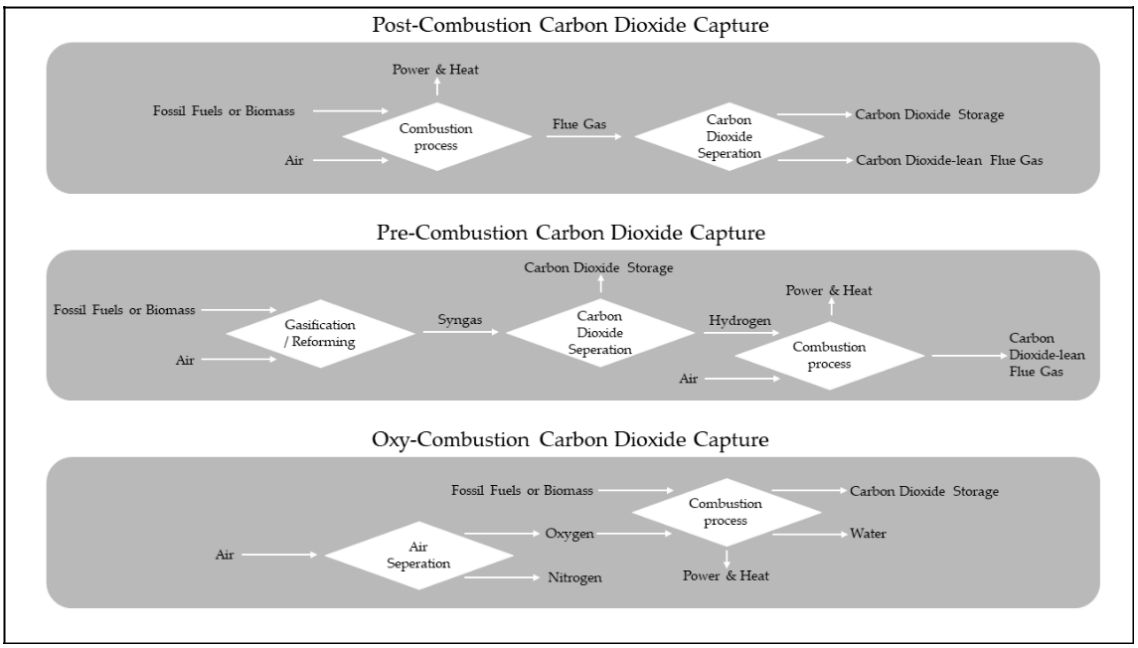

Figure 3: Basic systems of carbon dioxide capture (IEA, 2016)

The post-combustion system starts the process after conventional combustion that makes flue gas. This system focuses on the separation of the flue gas to isolate the carbon dioxide. In a pre-combustion system, the main focus lies on gasifying the fuels beforehand through oxygen-deprived combustion. The foundation for carbon dioxide separation lies in the created syngas. In the final system, oxy-combustion, the air is firstly separated to enable a combustion process with pure oxygen. Out of this combustion, only water and carbon dioxide come out as waste products. (Goel et al., 2018)

A capturing mechanism has to be present for this purpose. There are three essential mechanisms, which are (Metz, 2005):

- usage of a sorbent or solvent,
- usage of a membrane, or
- cryogenic distillation.

When a sorbent or solvent are used, carbon dioxide is fixed to the sorbent or solvent. In another vessel, carbon dioxide is separated from the same sorbent or solvent. This process typically requires energy. It may also consume a portion of the absorbent, and the remaining portion goes back to further capture carbon dioxide. This method does not need high pressure. On the other hand, a membrane does require higher pressures because a certain portion of carbon dioxide is trapped, and the other portion passes through the membrane. There are different kinds of membranes available, depending on the composition of the gas. Currently, there is no application of membrane capturing mechanism in large scale CCS projects. Same applies to cryogenic distillation, a system tried and tested in air separation. In this distillation, gas is liquefied in a series of compression, cooling, and expansion steps. As with membrane capture, cryogenic distillation also requires a massive flow of oxygen, which lowers the applicability in carbon capture and storage. An absorbent is the most frequent capturing method. The usage of absorbent creates economic implications, which is explained later. (Metz, 2005).

The most practical method of carbon dioxide transportation is by pipeline. When transporting carbon dioxide via pipeline, the phase of the CO_2 is crucial. Since gas has a low density, the transport would not be efficient in this case. The common state for efficient transportation is a dense phase liquid. For this state, a pressure of a minimum of 73.8 bar and a temperature of at least -56.6°C is required. When carbon dioxide is in conditions which are above its critical pressure, but below its critical temperature, the density increases as the temperature decreases. This characteristic is why carbon dioxide pipeline transport occurs within the dense phase liquid state. In this state, the density is similar to liquid, whereas the viscosity and compressibility are like in a gas. This phase also applies to the other modes of transport, like in a container of a ship, truck, or train. Because low temperatures are a necessity, cryogenic transport is the only option. Cryogenic conditions take up a lot of energy. Another issue would be the construction of a dedicated pipeline network. One such network exists within the United States, where carbon dioxide is in use as an enhanced oil or gas recovery method since the 1980s (Seevam et al., 2007).

2.1.1 CCS Potential

The CCS could offer serious potential in lowering carbon dioxide emissions and mitigate climate change. There are still some controversies regarding it. The most important one is the economic feasibility, followed by environmental considerations.

There are three types of geological formation which satisfy the criteria for storage. These are (Metz, 2005):

- depleted oil and gas reservoirs,
- coal beds which aren't minable,
- and deep salt formations.

In order for any of those to function as a carbon dioxide disposal site, a sealing cap rock has to be in place. Regarding coal beds and deep saline formations, they usually need to have a minimal permeability to be operated as a storage site. Depleted oil and gas fields have usually enough permeability to function as a storage site (Metz, 2005).

The technology which is necessary for storing carbon dioxide is the same as in the injection process in petroleum industry. From the required well with their monitoring methods to computer-added reservoir simulations, all of it is necessary for oil and gas exploration as well as carbon dioxide storage. Table 1 demonstrates the estimations of potential storage capacities of the eligible formations (Metz, 2005).

Type of Reservoir	Lower Estimation [Gigatons]	Higher Estimation [Gigatons]
Oil and Gas Fields	675	900
Unminable Coal Beds	3	200
Deep Saline Formations	1000	Up to 10.000

Table 1: Potential storage capacity of the eligible formations (Metz, 2005)

Based on the estimated capacities, it is possible to store the whole amount of annual carbon dioxide emissions. Based on 2012 data, this was estimated to be 36 gigatons. Unfortunately, the humanity is much faraway from having the ability to dispose the whole amount of generated carbon dioxide. There is an estimation which expects a storage of 8.2 gigatons annually in 2050. With extrapolated data to 2050, this corresponds to roughly 19% of the overall carbon dioxide emissions. This estimation was made by the International Energy Agency (IEA) (IEA, 2016).

In order for a geological formation to function as a storage site, it needs to have a trap with low permeability above it. This kind of trap usually exists in oil and gas reservoirs. These traps trap hydrocarbons and accumulate them in a reservoir below them. The seal is critical since carbon dioxide is buoyant in most subsurface settings and will migrate to the top point of the formation. For economic CCS operations, an injection rate of a minimum of one megaton carbon dioxide annually is necessary. Proper CCS operations inject multiple thousand tons of carbon dioxide per day (Metz, 2005).

It requires a well to inject carbon dioxide into a formation, often thousands of meters below the surface. Injection wells are common within the oil and gas industry and they made enhanced oil recovery already for many years possible. Carbon dioxide injection needs completion equipment which is resistant to corrosion. Injection wells may be constructed with various trajectories with the help of state of the art technologies. One injection well with a trajectory other than vertical (e.g. extended reach well) may be as effective as multiple vertical injection wells (Metz, 2005).

Phase of carbon dioxide is very important to make injection happen. Figure 4 shows carbon dioxide's phase diagram (Chegg, 2020).

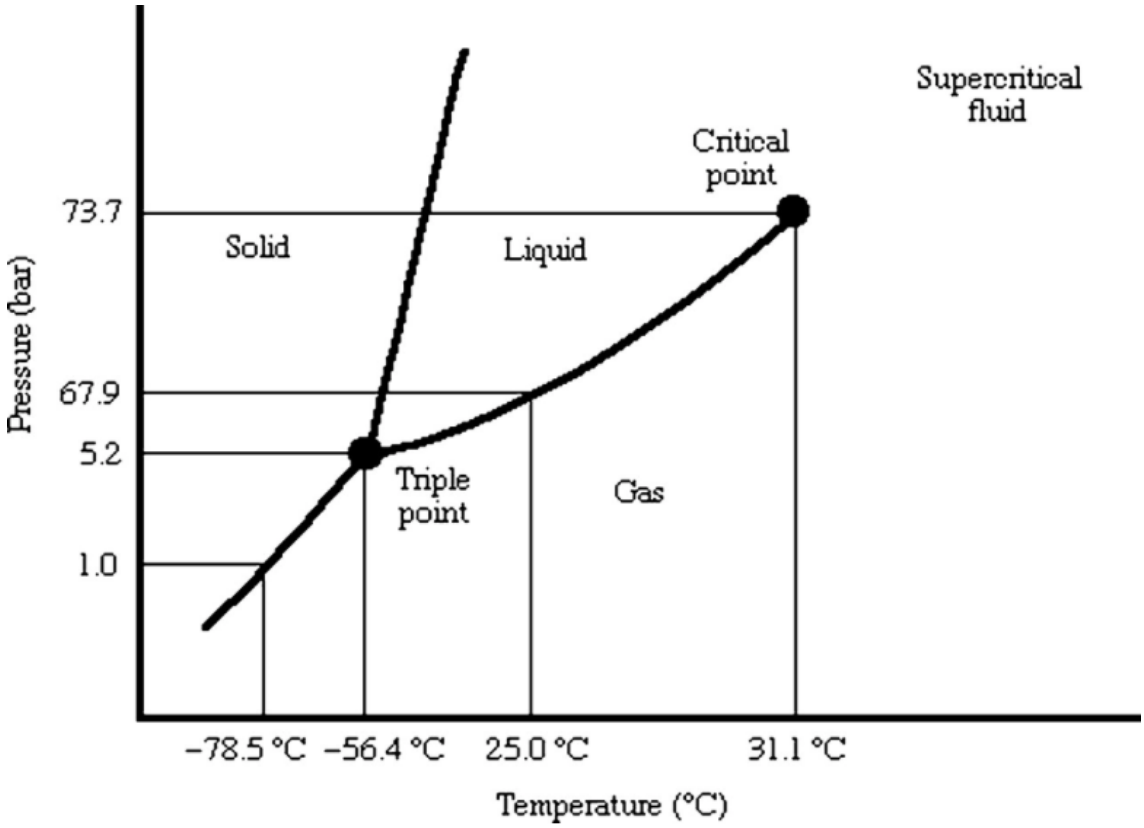

Figure 4: CO_2 phase diagram (Chegg, 2020)

When carbon dioxide is in the supercritical state, it has comparing to oil and water a fraction of their viscosity. At the triple point, supercritical carbon dioxide has a density of 1.8075 kg/m^3. The liquid density at the triple point is 1178.4 kg/m^3. Based on these properties, the liquid is the best option for transport. However, injection process needs other properties of carbon dioxide. Supercritical carbon may be mixed with natural gas. Inside the reservoir, it may form a stable front. The supercritical carbon dioxide isn't miscible in formation water. If there's no miscibility, the displacement depends on the density difference of the formation fluids and also the carbon dioxide. Regarding the miscibility with oil, this depends on the composition of the oil. Carbon dioxide is miscible with oil only in specific compositions. Fluid system behavior is completely different when the carbon dioxide is miscible with oil. When fluids are miscible, the forces of buoyancy are lower. Therefore, the vertical flow will be less. Also, the mixture of fluids will displace more in a radial way. A buoyant plume will form, nonetheless. As carbon dioxide migrates through a reservoir formation, there will always be a portion dissolved into water. That portion of carbon dioxide depends on water flow. This water flow has minimal velocities, starting from millimeters to centimeters per year. The water with dissolved carbon dioxide has a greater density compared to the formation water. Therefore, it migrates downwards. Consequently, formation water migrates upwards, leading to more carbon dioxide mixed with formation water. There were simulations conducted, which show that the migration of formation water mixed with carbon dioxide will become the leading displacement method (Air Liquide; Metz, 2005).

2.1.2 Economic Factors for CCS Projects

The determining factors of CCS for many corporations are economic factors. As opposed to enhanced oil or gas recovery, CCS doesn't currently create additional value. As legislations change, this might also change. One accepted theory is that governments are introducing fines or taxed on emitted carbon dioxide emissions. These taxes or fines may be off-put by storing the carbon dioxide within CCS projects and keeping it from discharging into the atmosphere.

The focus for the economic factors in this thesis is on the storage costs of carbon dioxide in geological formations. Costs resulting from capture, compression, and transport are neglected.

The three factors, which determine the cost of storage are:

- construction of the well,
- well infrastructure and,
- administrative and management costs.

Constructing a well for CCS enables additional considerations within the planning phase in terms of carbon dioxide resistance. Cost of storage is much higher than the application of existing oil and gas well. Regarding safety aspects, existing oil and gas wells set a greater risk compared to new wells. The reason for it is that Portland cement is not resistant on carbon dioxide. Table 2 breaks down the carbon dioxide storage costs (Allison et al, 2003, Bock et al., 2003, Hendrick, Crijns-Graus, Bergen, 2004).

Option Type	Onshore or Offshore	Location	US$/t Carbon Dioxide Stored		
			Low	Mid	High
Saline Formation	Onshore	Australia	0.2	0.5	5.1
Saline Formation	Onshore	Europe	1.9	2.8	6.2
Saline Formation	Onshore	USA	0.4	0.5	4.5
Saline Formation	Offshore	Australia	0.5	3.4	30.2
Saline Formation	Offshore	North Sea	4.7	7.7	12
Depleted Oil Field	Onshore	USA	0.5	1.3	4
Depleted Gas Field	Onshore	USA	0.5	2.4	12.2
Disused Oil or Gas Field	Onshore	Europe	1.2	1.7	3.8
Disused Oil or Gas Field	Offshore	North Sea	3.8	6	8.1

Table 2: Storage costs of carbon dioxide based on different studies
(Allison et al, 2003, Bock et al., 2003, Hendrick, Crijns-Graus, Bergen, 2004)

Well construction has the greatest influence on storage costs. The costs of a new injection well may range from 200,000 United States Dollars (onshore) until 25 Million United States Dollars (offshore). Recompleting existing wells can be a much cheaper option. Of course, depth is also an influence factor, since well construction and compression costs increase with depth. What may also lower costs it to permit a certain composition of impurities of carbon dioxide. Greater amount of impurities lower costs when carbon dioxide is captured, but these impurities (NO_x, H_2S, SO_x) increases costs of completion. This is because these impurities have corrosive properties. Feasibility is finally determined on balancing the amount of impurities, depending on cost reduction and the total amount of impurities (Bock et al., 2003, Hendrick, Crijns-Graus, Bergen, 2004).

2.1.3 Utilization of Carbon Dioxide in EOR Operations

An oilfield has various phases of production in its life cycle. After the primary and secondary recovery phase, there is still roughly 65% of the original oil in place. Tertiary recovery methods enable further production of the oil that is still in the reservoir. One of such tertiary recovery methods is the utilization of carbon dioxide. This method is in use since the 1970s. Miscibility with oil is necessary. This is because with it, it changes the wettability properties. With it, tertiary production may be achieved. Supercritical

carbon dioxide is entirely miscible in most oils. Out of the total well production, this type of recovery accounts for 17% of it. It is important to note that storage of carbon dioxide in a geological formation is a beneficial side effect of enhanced oil recovery (EOR) and enhanced gas recovery methods. With this in mind, EOR projects don't enable long-term carbon dioxide storage. Carbon dioxide is used in EOR projects as long as it economically feasible to cover all the respective costs (Institute for 21st Century Energy, 2012).

The key to successful enhanced oil recovery using carbon dioxide is the miscibility of carbon dioxide with oil. The light components of oil are completely miscible. On the other hand, heavy components are not miscible with carbon dioxide. Assuming a well is a candidate for EOR operations using carbon dioxide, two commonly used injection strategies exist. A requirement to choose the correct injection strategy is a thorough understanding of the reservoir pressure. In an ideal case, a continuous injection of carbon dioxide gives the best results. Within this method, zones form within the reservoir. The order of the zones from injector to the production well would be the following (Saini, 2017):

- Carbon dioxide zone,
- Miscible zone (carbon dioxide combined with oil),
- Oil slug and,
- Pure oil zine.

Between these zones are transition zones, which range from either pure oil or carbon dioxide to the thorough mixed fluid. Continuous flow of carbon dioxide is a good strategy also in regard to storage efficiency. Another strategy includes a period of carbon dioxide injection, followed by water injection. This strategy is called a water alternating gas (WAG) strategy. The period when injection of water or carbon dioxide occurs may last from one month until up to a year. After that period, the change of injection fluid occurs and goes for the same period of time. The water injection reduces mobility of carbon dioxide in the formation, which prevents channeling. Regarding this strategy, the storage efficiency of carbon dioxide is lower compared to the continuous carbon dioxide injection. The reason for it is an obvious one. During the water injection, there is no carbon dioxide injection happening. This enhances the fact that carbon dioxide in EOR projects is only used for an increase of oil and gas production (Saini, 2017).

It is common for the purpose of EOR projects to buy carbon dioxide in big amounts. In some cases, point sources may supply EOR projects with carbon dioxide. However, the standard case is to buy it from manufacturers. The economic aspects of the operation depend on the oil price and the carbon dioxide price. The carbon dioxide price is tied to the oil price. In the United States, a West Texas Intermediate (WTI) price of 25 US$ per barrel represents a carbon dioxide price of 16.3 US$ per ton. Revenues from oil production have to compensate for the increased expenses due to carbon dioxide purchase. These expenses are quite significant in EOR projects since, on average, they account for 68% of the total costs. Based on calculations, for every barrel of oil between 0.15 and 0.4 tons of carbon dioxide is required. As EOR is not designed as a storage project, part of carbon dioxide which was injected into the reservoir comes back on the surface with produced oil. At the surface, separators split it from the oil and the separated carbon dioxide is reinjected into the reservoir (Bock et al.,2003; Metz, 2005).

2.2 Carbonation

As explained before, when carbon dioxide is stored in a geological formation or utilized in enhanced oil recovery, the carbon dioxide is typically injected in its liquid state. In reservoir conditions, the carbon dioxide will be usually in a supercritical state of aggregation. The reason for it is that almost all reservoirs exceed the critical point of carbon dioxide. The critical point of it has a temperature of 31.1°C and a pressure 73.8 bar. The greatest issue is the cement carbonation. This occurs due to a chemical reaction of calcium phases within Portland cement together with carbon dioxide. The main topic for this thesis is the monitoring of the carbonation process in real-time. It is of a great importance to monitor and understand the carbonation and its progression since it can have deteriorating effects on the cement and well integrity.

2.2.1 Composition of Portland Cement

Portland cement is typically applied for well cementing operations. It belongs to the group of hydraulic cements, which develop compressive strength under hydration. In this process, water and cement components make a reaction.

According to the American Petroleum Institute (API), Portland cement is categorized into various classes and grades. They regulate cement's chemical composition. The most popular cement is Class G cement, which is defined by the API as follows (API RP 10A, 2002):

''The product obtained by grinding Portland cement clinker, consisting essentially of hydraulic calcium silicates, usually containing one or more forms of calcium sulfate as an interground additive. No additives other than calcium sulfate or water, or both, shall be interground or blended with the clinker during manufacture of Class G well cement. This product is intended for use as a basic well cement. Available in moderate sulfate-resistant (MSR) and high sulfate-resistant (HSR) Grades.''

Table 3 shows the chemical composition of Class G cement. (API RP 10A, 2002)

High-Sulfate Resistant API Class G Cement	
Magnesium Oxide (MgO), maximum, %	6.0
Sulfur Trioxide (SO_3), maximum, %	3.0
Loss on Ignition, maximum, %	3.0
Insoluble Residue, maximum, %	0.75
Tricalcium Silicate (C_3S), maximum, %	65
Tricalcium Silicate (C_3S), minimum, %	48
Tricalcium Aluminate (C_3A), maximum, %	3
Tetracalcium Aluminoferrite (C_4AF) plus twice the Tricalcium Aluminate (C_3A), maximum, %	24
Total Alkali Content expressed as Sodium Oxide (Na_2O) equivalent, maximum, %	0.75

Table 3: Chemical composition for API Class G high-sulfate resistant cement (API RP 10A, 2002)

Along with chemical composition, the physical properties are also taken in this standard. Physical properties are guaranteed with the proper amount of water mixed with cement. Along it, the curing conditions and time are also important to comply to the standard. In this standard, the minimum compressive strength is also mentioned.

2.2.2 Portland Cement Hydration

This section has a focus on chemical reactions within the hydration process of the cement. It will cover the aluminate and clinker phases. It is necessary to understand the hydration mechanism because then the understanding and monitoring the carbonation of the cement may happen.

Regarding the clinker phase, not all aspects of the hydration is even nowadays completely understood. As tricalcium silicate (C_3S) is the most important component, the hydration of it will be discussed in this section. It also has a great influence on cement hardening. Dicalcium silicate (C_2S) is also important, but it behaves similarly to C_3S so the hydration of C_2S won't be presented here. Hydration is divided into five periods based on the readings of calorimeter. Figure 5 shows these five distinctive periods (Nelson and Guillot, 2006).

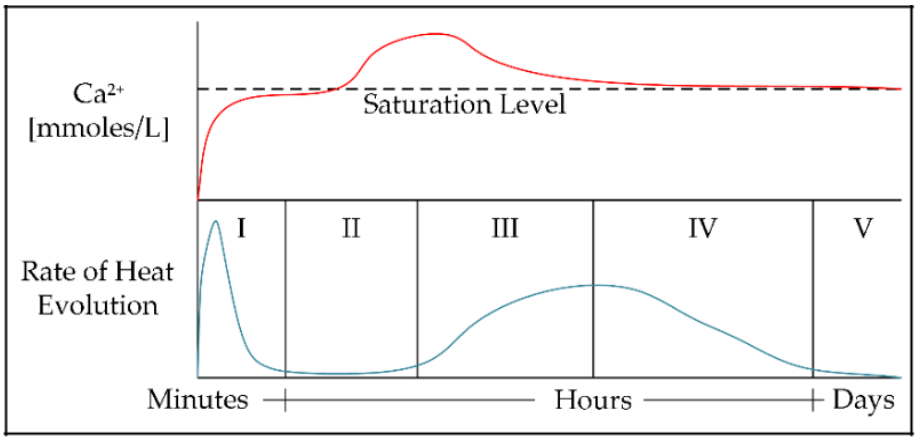

Figure 5: Showcase of hydration periods for clinker phase hydration (Nelson and Guillot, 2006)

The first period is also called the preinduction period. This period starts when the cement powder is mixed with water. Preinduction period lasts for a few minutes. A considerable heat output defines this period. This happens because of quick initial hydration of the cement powder. During this period, O^{2-} ions go into the liquid phase as OH^- ions and SiO_4^{4-} ions form silicic acid, as seen in Equation 1 (Barret, 1986).

$$2Ca_3SiO_5 + 8H_2O \rightarrow 6Ca^{2+} + 10OH^- + 2H_3SIO_4^- \quad (1)$$

As the C_3S reaction occurs quicker compared to the dissipation of the surface products, a layer of a calcium silicate hydrate (C-S-H) phase starts forming at the surface. This is also seen in Equation 2 (Barret, 1986).

$$2Ca^{2+} + 2OH^- + 2H_3SIO_4^- \rightarrow Ca_2(OH_2)H_4Si_2O_7 + H_2O \quad (2)$$

When Equation 1 and Equation 2 are combined, they give the overall reaction within the preinduction period. Equation 3 shows this combination (Nelson and Guillot, 2006).

$$2Ca_3SiO_5 + 7H_2O \rightarrow Ca_2(OH_2)H_4Si_2O_7 + 4Ca^{2+} + 8OH^- \quad (3)$$

The second period in the clinker phase hydration is called the induction period. After the initial exotherm, the dissipated heat declines back to zero, as seen in Figure 5. The period of zero heat dissipation is the induction period. While this period occurs, the precipitation of C-S-H phase slowly continues, and the Ca^{2+} and OH^- concentrations increase. The actual process which occurs during this induction period is still subject to discussion among cement scientists. There are multiple theories which exist. This section will cover only the impermeable hydrate layer theory (Nelson and Guillot, 2006).

This theory assumes, that because of the slower speed of dissipation of the Equation 1 products in comparison to the speed of reaction, an impermeable layer generates at this surface. It also prevents migration of water to the reactants which are not hydrated. It also prevents Ca^{2+} and OH^- from going into the liquid phase. The halt of an initially fast reaction is caused by the formation of the impermeable layer. In room temperature conditions, the induction period takes a few hours. After this period, the C-S-H layer gains more permeability. Also, the hydration rate accelerates, which may be notices with a rise in dissipated heat (Brown et al., 1984).

When the first two periods end, a small amount of C_3S has hydrated. Most hydration occurs in the setting period. The setting period may be further divided into acceleration and deceleration period. In the acceleration period, Portlandite crystals form (the chemical composition of them being $Ca(OH)_2$) and the C-S-H phase occupies the remaining space, filled with water up to now. Acceleration period takes pore space away. This leads to reduction of porosity. After a certain point in time, the hydration can no longer increase because the available pore space is insufficient. This moment is also a transition from acceleration period to deceleration period. The setting period also generates the strength of the cement (Nelson and Guillot, 2006).

The final period of this process is the diffusion period, which is not strictly separated with the deceleration. While the deceleration period may last only a few days, the diffusion period may be indefinite. Cement porosity slowly decreases further, which slows down further the hydration process. With this the cement density and compressive strength increase. During this period, Portlandite crystals entrap non-hydrated C_3S phases. Because of this, total hydration can never be achieved (Glasser et al., 1978).

That other phase which will be described in this thesis is the aluminate phase. The aluminate phases (C_3A and C_3AF) show far more hydration at short times. Aluminate phase gives to the cement the rheological properties. As in the clinker phase, the hydration of C_3A is similar to that of C_3AF. For that reason, this section only illustrates the hydration of C_3A in detail (Nelson and Guillot, 2006).

Initial step of this reaction is the mixture process of water with the anhydrous surface of the solids. This process is similar to the hydration of C_3S. Hydration of the aluminate phase creates aqueous ions in solution at the surface. This is seen in Equation 4 (Barret, 1986).

$$Ca_3Al_2O_6 + 6H_2O \rightarrow 3Ca^{2+} + [Al(OH)_4]^- + 4OH^- \quad (4)$$

These ions reach quickly the saturation level in the solution. It causes the precipitation of calcium aluminate hydrates. This is shown in Equation 5 (Nelson and Guillot, 2006).

$$6Ca^{2+} + 4[Al(OH)_4]^- + 8OH^- + 15H_2O \rightarrow$$
$$Ca_2[Al(OH)_5]_2 * 3H_2O + [2Ca_2Al(OH)_7 * 6H_2O] \quad (5)$$

Combining Equation 4 and 5, hydration of the aluminate phase and formation of calcium aluminate hydrates is made. Equation 6 depicts this sum (Nelson and Guillot, 2006).

$$2Ca_3Al_2O_6 + 27H_2O \rightarrow$$
$$Ca_2[Al(OH)_5]_2 * 8H_2O + [2Ca_2Al(OH)_7 * 19H_2O] \quad (6)$$

The calcium aluminate crystals from Equation 6 materialize in a hexagonal crystal structure. At laboratory conditions, typically in several days, the react to form the more stable C_3AH_6, which has a cubic crystal structure. Equation 7 shows this transformation (Tumidajski and Thomson, 1994).

$$Ca_2[Al(OH)_5]_2 * 8H_2O + [2Ca_2Al(OH)_7 * 19H_2O$$

$$\rightarrow 2Ca_3Al_2^{3+}(OH)_{12} + 27H_2O \quad (7)$$

Silicate ions usually renew the charge imbalance in the cubic calcium aluminate crystal. This results in the formation of Katoite ($Ca_3Al_2[(SiO_4)_{3-x}(OH)_{4x}]$). When all charges are balanced, the Katoite is in stable form. X may range from 1,5 to 3. When x is equal to 3, then the form is stable (Anthony, 1995).

2.2.3 Portland Cement Carbonation

During cement hydration, a free fluid is created. This means that around 0.6% of water migrates out of the slurry. After migration, it stays on the slurry surface. When cement is exposed to the carbon dioxide, carbonation process starts. It may destroy the cement integrity. This is done with the increase of porosity and reduction of compressive strength. Cement porosity is the main driver for carbonation. When carbon dioxide cannot go through the cement pores, it can only affect the surface area of the cement. For EOR projects, the cement mixture which may be resistant to carbonation is too expensive to be viable. When carbon dioxide is in reservoir conditions, it is in the supercritical state of aggregation. In this state, it requires less porosity of the cement for surface penetration. Liquid carbon dioxide needs to have a greater cement porosity in order to penetrate the cement slurry (Nelson and Guillot, 2006).

Carbonation is initiated with the reaction of carbon dioxide with water. This reaction forms the carbonic acid. Water may appear in form of a free fluid or as a water which is left over from the cement hydration process. Equations 8 to 10 illustrate the main steps of this process (Onan, 1984; Bruckdorfer, 1986).

$$CO_2 + H_2O \leftrightarrow H^+ + HCO_3^- \leftrightarrow H_2CO_3 \quad (8)$$

$$Ca(OH)_2 + H^+ + HCO_3^- \rightarrow CaCO_3 + 2H_2O \quad (9)$$

$$C-S-H \text{ phase} + H^+ + HCO_3^- \rightarrow CaCO_3 + \text{amorphous silica gel} \quad (10)$$

In this thesis, a sandstone kept at laboratory conditions mimics the geological formation. For the experiments run in this thesis, the goal was to establish slurry composition which would give as less free fluid as possible. In ideal case, this would be a free fluid content of 0%. When carbonic acid is diffused into the cement pores, the ions which are disassociated react with calcium hydroxide and the C-S-H phase. This reaction forms new equilibria, what is demonstrated in Equation 11 and Equation 12 (Bruckdorfer, 1986).

$$CO_2 + H_2O + CaCO_3 \rightarrow Ca(HCO_3)_2 \quad (11)$$

$$Ca(HCO_3)_2 + Ca(OH)_2 \leftrightarrow 2CaCO_3 + 2H_2O \quad (12)$$

Because the carbon dioxide is in an abundant amount in reservoir conditions, calcium carbonate reacts with calcium bicarbonate. Calcium bicarbonate may move out of the cement when it is dissolved in the water. Reaction of calcium hydroxide and calcium bicarbonate generate water and calcium carbonate. This is also the reason why carbonation is reducing the integrity of the cement. When water is formed, the bicarbonate is dissolved and it may move out of the cement. Consequently, porosity of the cement is increased and compressive strength is reduced. This leads ultimately to the loss of well integrity. High temperatures favors also the carbonation process. Additives are required to prevent this process (Bruckdorfer, 1986).

Chapter 3 Methods of Monitoring Carbonation

To study the effect of carbonation, multiple test methods have to be introduced. This is a necessity to make the monitoring of this process continuous. For the purpose of this thesis, there are two methods which are going to be used. These non-destructive monitoring methods are the following:

- acoustic method,
- computer tomography (CT) scanning.

To confirm the monitoring measurements, destructive tests are also used in order to correlate and verify the non-destructive test methods. These are:

- Uniaxial compressive strength (UCS) test,
- Brazilian test,
- Scanning Electron Microscopy (SEM) and,
- X-ray Diffraction (XRD) method.

The acoustic method is also the area of special interest for this thesis. It is one of the non-destructive monitoring methods which already has a wide application in the evaluation of concrete.

3.1 Acoustic method

Acoustics define the propagation of sound waves in the media. There is also a subsection important for this thesis. This is ultrasonic, which covers all sound waves with a frequency of at least 20 kHz. That kind of waves allows the conduction of non-destructive tests. These kind of tests make no damage to the material, but material properties may be determined with it. For the aim of this thesis, piezoelectric material is applied in order to provide the acoustic waves which are going to be measured and evaluated for the compressive strength of the cement.

3.1.1 Physical Properties of Acoustic Measurement

In 1880 the Curie brothers discovered the piezoelectric behavior of certain materials. These materials generate an electrical charge at their surface when subjected to mechanical stress. In 1881, they also discovered the inverse piezoelectric effect. What this implies is when a piezoelectric material is subjected to an electrical charge, it will change its form. These two effects are the foundation for ultrasonic analysis using piezoelectric sensors. Same piezoelectric element can be used in two ways. One way is that it functions as a transmitter and the other is that it functions as a receiver. The difference between these functions is the application of an electric charge. The transmitter applies the input charge. The receiver measures then the output electric charge. A piezoelement does not have a center of symmetry in its crystalline structure. The presence of such a center of symmetry often depends on the temperature. Lead zirconate titanate (PZT) is used as

the applied piezoelectric material (Krautkrämer, Krautkrämer, 1990). A simplified version of the piezoelectric element is shown in Figure 6. (Rupitsch, 2019)

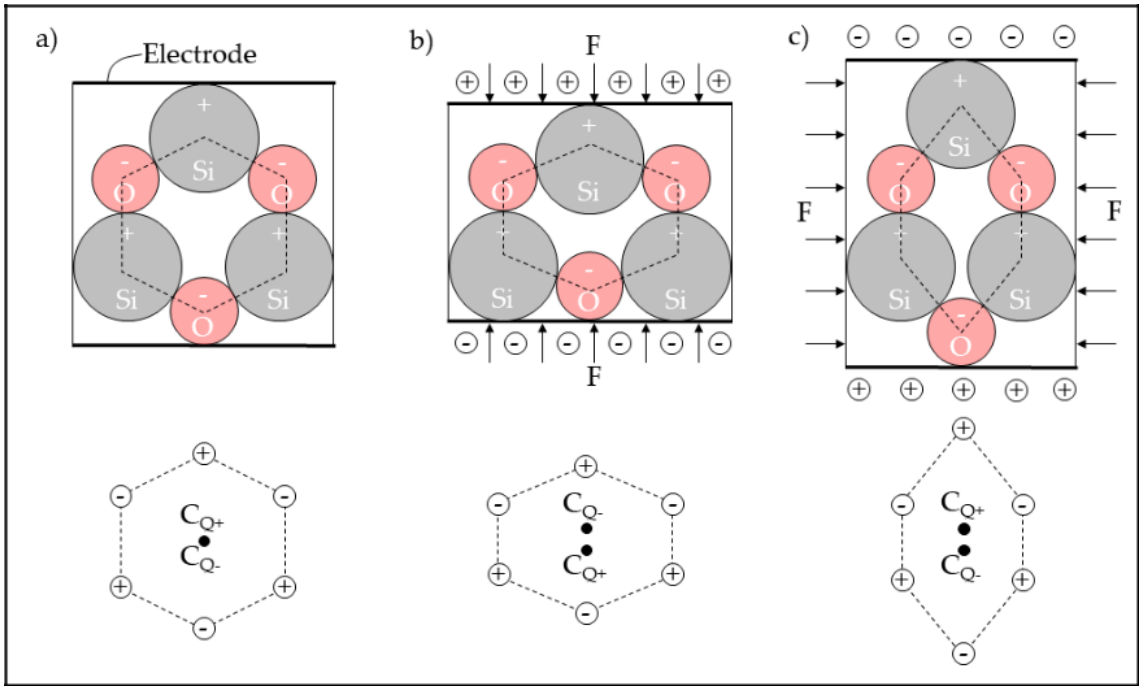

Figure 6: Simplified quartz crystal structure (Rupitsch, 2019)

A quartz crystal only consists of the elements silicon (Si) and oxygen (O). Electrodes are set into the top and bottom surface of this crystal. In the first state (a), the charges are balanced. C_{Q+} and C_{Q-} indicate the center of the positive and negative charges, respectively. In this state, the crystal is neutral. The centers are in the same geometric position. A force (F) causes changes in the balance in the second (b) and third state (c). Because of it, the centers of charge are no longer in the same geometric position. This change of state creates a dipole, which creates electric polarization. Polarization is affected by the distance between the centers of charge. In order to offset the imbalance which occurs internally, the crystal creates an electric charge in the electrodes (Rupitsch, 2019).

The piezoelectric element applied for this thesis is a modified PZT. This type of PZT is also called PIC255. As the PZT is modified, this means that crystals are doped with ions of other element. These elements may be Nickel, Bismuth, Niobium etc. The doping process allows optimization of piezoelectric characteristics of the selected material. The most critical aspect is Curie Temperature. When above it, the material loses its piezoelectric properties. Below it, crystal structures of the material are asymmetrical. This asymmetrical structure generates a formation of dipole. In this case, the Cure Temperature is between 200 and 350°C. The operating temperature should be between -20 and 150°C (PI Ceramic GmbH, 2020). The piezoelectric element is shown in Figure 7.

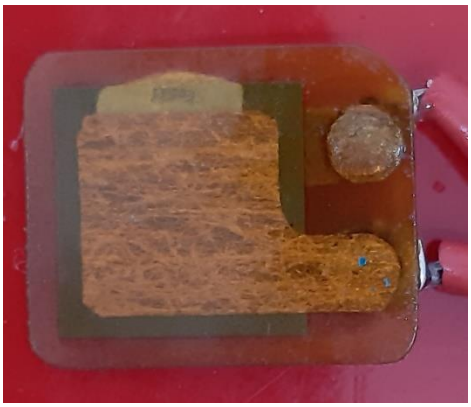

Figure 7: Piezoelectric element used for the Thesis

Utilizing the inverse piezoelectric effect, the elements emit ultrasonic waves. In this setup, a generator creates the input function. The amplifier makes the function to be at a higher voltage. That amplified function is then carried to the piezoelectric element. Electrodes deliver the electric energy to the piezoelement. This electric energy is turned into mechanical energy within the element. The ultrasonic waves are then emitted. Two or three elements create the sensing arrangement. One will generate the ultrasonic waves, while the other elements receive reflected and refracted waves from the transmitting piezoelectric sensor.

The body waves travel within the body of a solid material. These body waves are the pressure waves, also called P-waves, and also the shear waves, also referred to as S-waves. There are surface waves, also called Raleigh waves or R-waves, which travel along the free surface of the material. The velocities of wave propagation depend upon elastic constants and the mass density of the material. The relations among P-wave, S-wave, and R-wave velocities can be expressed through Equation 13 to Equation 15 (Lee, Oh, 2016):

$$v_p = \sqrt{\frac{E_d\,(1-v_d)}{\varphi\,(1+v_d)(1-2v_d)}} \tag{13}$$

Where:

- v_p is the P-wave velocity [m/s],
- E_d is dynamic Young's modulus [Pa],
- v_d is dynamic Poisson's ratio and [-],
- φ is density [kg/m^3].

$$v_s = \sqrt{\frac{E_d}{\varphi\, 2(1+v_d)}} \tag{14}$$

Where v_s is the S-wave velocity [m/s].

$$v_R = \frac{0.87+1.12v_d}{(1+v_d)} \sqrt{\frac{E_d}{\varphi\, 2(1+v_d)}} \tag{15}$$

Where v_R is the R-wave velocity [m/s].

P-wave velocity typically ranges from 3500 m/s to 4500 m/s and the surface wave velocity range from 1800 to 2500 m/s for sound concrete. The motion resulting from R-waves is restricted to an area near the surface and reduces exponentially in amplitude away from the surface. The R-wave penetration depth is inversely associated with the frequency of the wave. As R-waves have a larger amplitude, they may be easier to sense. The constraint of the R-waves is the limited depth of penetration. P-wave velocity is commonly used for measurement. As the energy of P-wave is the lowest, it is harder to make the experimental data stable in statistical sense. Furthermore, the P-wave depends on the presence of pore water within the concrete (Lee, Oh, 2016).

When a wave is coming to the edge of one material and on the beginning of the other, the whole portion of the wave won't pass through the interface. One portion of the wave will be reflected into the first material. The rest of the wave will transmit into the other material. Acoustic impendance determine the portions of the reflected and transmitted wave. When the difference between the impendances is greater, then the bigger portion of the wave is going to be reflected. Angle is the original wave is going to be the same as the angle of the reflected wave. This is defined with the Snell's law. Figure 8 showcases the Snell's law in practice. This is further demonstrated with the Equation 16. (Burrascano et al, 2015).

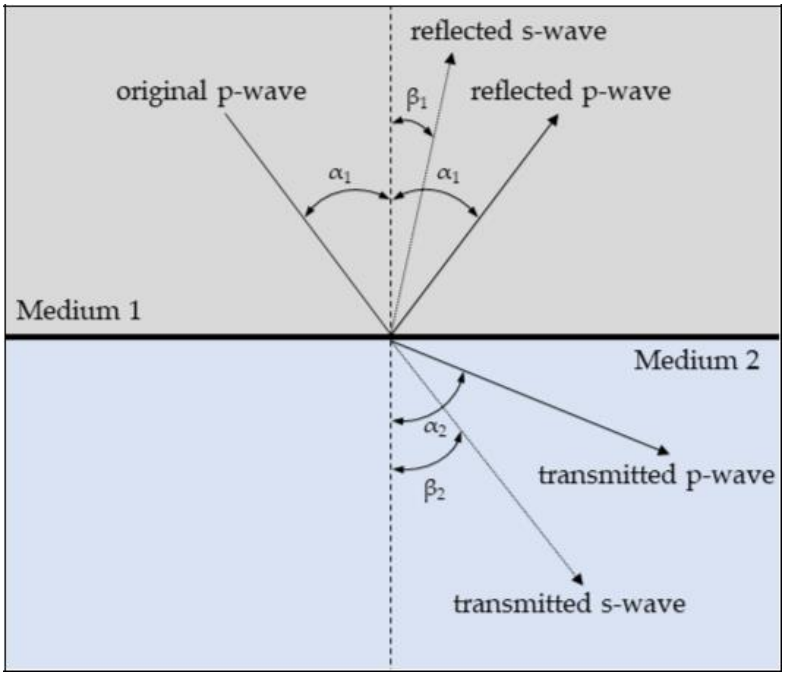

Figure 8: Graphical showcase of Snell's law (Burrascano et al., 2015)

$$\frac{v_{p1}}{\sin_{\alpha 1}} = \frac{v_{s1}}{\sin_{\beta 1}} = \frac{v_{p2}}{\sin_{\alpha 2}} = \frac{v_{s2}}{\sin_{\beta 2}} \tag{16}$$

Where:

- v_{p1} is the P-wave velocity in the first medium [m/s],
- v_{s1} is the S-wave velocity in the first medium [m/s],
- v_{p2} is the P-wave velocity in the second medium [m/s],
- v_{s2} is the S-wave velocity in the second medium [m/s],
- $\sin_{\alpha 1}$ is the sine of the angle between the reflected P-wave direction and the interface [-],
- $\sin_{\beta 1}$ is the sine of the angle between the reflected S-wave direction and the interface [-],
- $\sin_{\alpha 2}$ is the sine of the angle between the transmitted P-wave direction and the interface [-],
- $\sin_{\beta 2}$ is the sine of the angle between the transmitted S-wave direction and the interface [-].

Three forms of interfaces occur within the setup for the cement analysis. The first type is the interface between the transducer and receiver and also the cell holding the cement. This interface is vital, since a lousy coupling here, can result in a loss of most of the energy. Second interface is between materials within the autoclave. Third interface are the damages within materials. This may reflect the ultrasonic waves.

Poisson created an equation for the portions of reflected and transmitted waves. The result of the equation depends on the acoustic impendance of the respective materials. The equations are shown in Equation 17 and Equation 18 (Burrascano et al., 2015).

$$R = \frac{Z_2 - Z_1}{Z_2 + Z_1} \quad (17)$$

Where:

- R is the reflected portion of the waves [-],
- Z_1 is the acoustic impedance of the first material and [kg/m²s],
- Z_2 is the acoustic impedance of the second material [kg/m²s].

$$T = \frac{2Z_2}{Z_2 + Z_1} \quad (18)$$

Where T is the transmitted portion of the waves [-].

An example of these factors is the interface between water and steel. Steel has an acoustic impedance of $45*10^6$ kg/m²s and water has an acoustic impedance of $1.5*10^6$ kg/m²s. Using these values in the previous two equations, where the steel acoustic impedance takes the value of Z_1 and water acoustic impedance takes the value of Z_2, the equations deliver the following results:

- R=0.935 and,
- T=0.065.

This means that 93.5% of the waves are reflected and only 6.5% are transmitted further (Krautkrämer, Krautkrämer, 1990).

3.1.2 Application of ultrasonic pulse velocity in concrete measurement

The ultrasonic pulse velocity (UPV) is in application for quality of concrete. It has been applied for already more than 60 years. It may be used to detect defects within the concrete. One example would be to detect internal cracks. By using the pulse velocity method, it's also possible to estimate the strength of concrete test specimens. As this is a non-destructive test method, it may be measured with an infinite number of times (Naik et al., 2004).

With the help of UPV, the compressive strength of concrete may be estimated. However, there is no physical correlation between sonic velocity and compressive strength. Compressive strength is determined with a graph. This graph links the compressive strength and sonic velocity of the material. The link between these 2 parameters is not unique. It may be affected with a lot of factors regarding the content of concrete. Therefore, correlation between compressive strength and sonic velocity has to be determined in advance. Figure 9 shows an example of such a relationship (Naik et al., 2004).

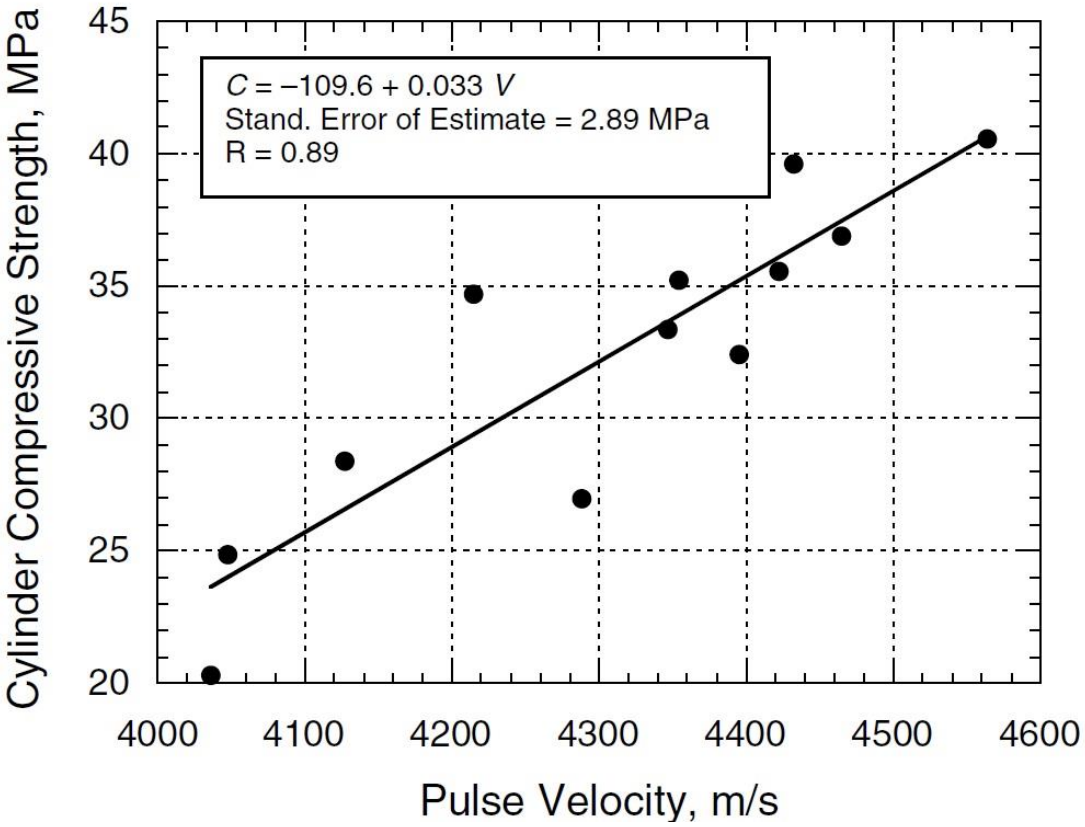

Figure 9: Sample correlation between pulse velocity and compressive strength (Naik et al., 2004)

As the structure of cement is damaged, the sonic velocity is being reduced. Damage may be caused by a lot of factors, such as freezing or corrosion of embedded items. The damage may be detected with the help of UPV method. Continuous measurements enable to detect progressive deterioration (Naik et al., 2004). This can be also applied for the carbonation process of the cement because the porosity is increased, and the compressive strength is reduced because of that process.

When a sonic wave comes to a crack which is filled with air, the wave will travel around the crack. Thus, the pulse travel time will be longer than the travel time through similar concrete without any kind of defect. The UPV method, therefore, is effective in characterizing surface cracks. Application of this technique has also constraints. For example, a crack which is too small may not be detected. Another example would be a crack filled with water, which won't reduce the sonic velocity as much as the air filled crack. The depth of an air-filled surface crack can be estimated by the UPV method as shown in Figure 10. The depth of the crack is given by the Equation 19 (Naik et al., 2004).

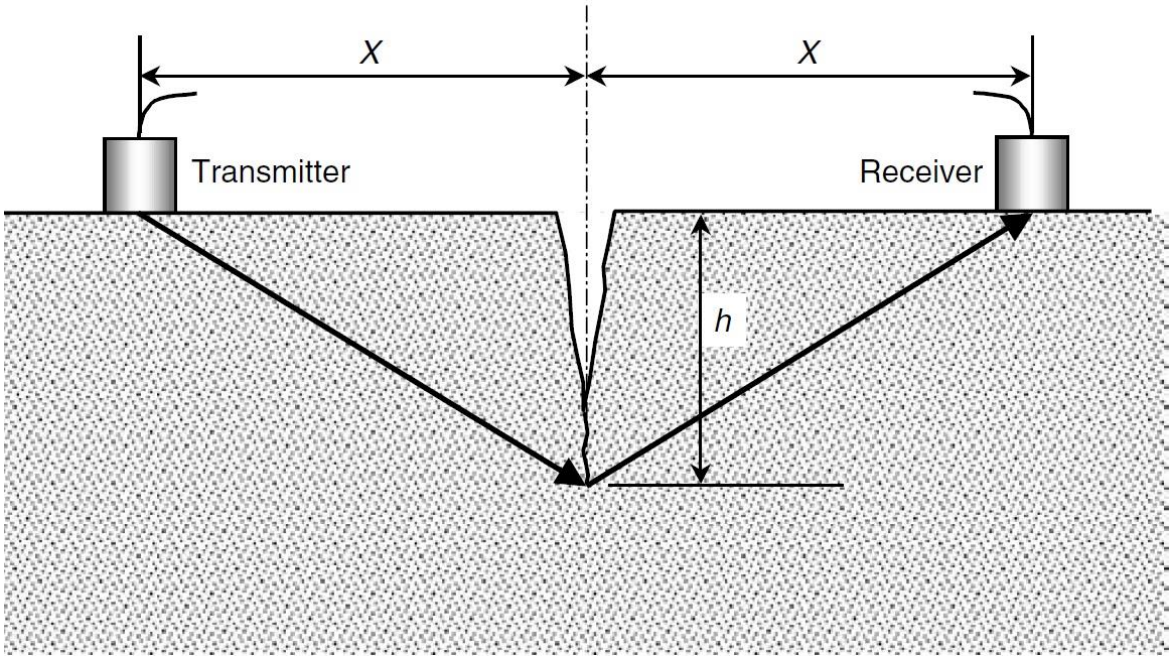

Figure 10: Scheme for measurement of surface crack depth (Naik et al., 2004)

$$h = \frac{x}{t_2}\sqrt{t_1^2 + t_2^2} \quad (19)$$

Where:

- h is the crack depth [m],
- x is the distance between crack and transducer [m],
- t_1 is the travel time around the crack [s] and,
- t_2 is the travel time along the surface of the same type of concrete without any damage [s]

Other areas of application where the ultrasonic pulse velocity method is used are the following (Naik et al., 2004):

- Determination of dynamic modulus of elasticity,
- Determination of cement hydration and,
- Measurement of concrete homogeneity.

Two other works are presented here to gain a better picture of UPV application. Kalyan and Kishen did a research with the portable ultrasonic non-destructive digital indicating tester (PUNDIT) to determine the effect of cracks on sonic velocity. When material doesn't have any defect, the sonic velocity travels faster through it. By calculating that velocity, the properties of the structural concrete may be assessed. For the experimental process, four concrete cubes of dimensions 150x150x150 mm with different concrete strengths were casted. One cube was loaded up to 45% of its compressive strength. The other cube was loaded up to 65% of its compressive strength. The loading of both of the cubes resulted in formation of internal micro cracks. The undamaged cube which is taken as a reference in this research has a compressive strength of 25 MPa.

Three different types of probing methods were used and there were the following (Kalyan and Kishen, 2014):

- Direct Probing (case a),
- Surface Probing (case b) and,
- Semi direct Probing (case c).

The setup of each probing method is shown in Figure 11 (Kalyan and Kishen, 2014).

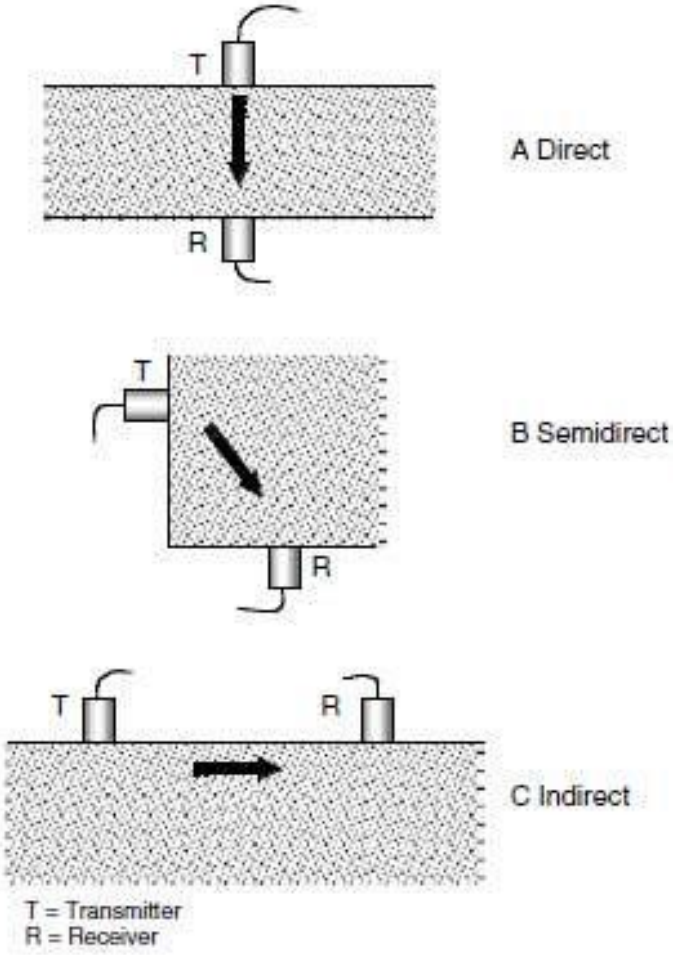

Figure 11: Position of probes for probing (Kalyan and Kishen, 2014)

In the first case, the cube which was loaded with 45% of its compressive strength, the elastic modulus did not change much from the undamaged cube. In the other case, the cube which was loaded with 65% of its compressive strength, its elastic modulus got reduced by 50% compared to the undamaged sample. This means that the internal cracks developed in the first cube do not affect significantly the sonic velocity. In other case, the path of the waves may change, so it can affect the sonic velocity in a greater way. Also, surface cracks are developed in the second case. The surface cracks have a great effect on sonic velocity. Therefore, the UPV is not affected by micro cracks. The measurement of the elastic modulus and compressive strength needs to be measured with a more sensitive method compared to the UPV (Kalyan and Kishen, 2014).

There is also a case where a notch is developed. The purpose of it is to study surface cracks and how do they affect the sonic velocity. A notch in this case has a width of 4 mm and a depth of 50 mm. Direct probing and Surface probing are used in this case to determine the effect of the notch. When direct probing is applied, the notch effect is nonexistent. For this, the sonic velocity does not change. In case of surface probing, there is a drastic change in sonic velocity, therefore the surface probing is the preferred probing method to evaluate surface cracks. Calculations were also made based on Equation 19 and it was observed that there is a great difference between calculated and true crack depth. Thus it can be said that the wave path cannot be approximated to a straight line without any constraints. Based on the results, it can be said that UPV can be employed for the detection of cracks and for evaluating their effects, but this cannot be solely used and should be accompanied by other non-destructive test methods for better accuracy and identification of the cracks and evaluation of the properties of concrete. (Kalyan and Kishen, 2014)

Baehaki and al. also applied PUNDIT to determine the crack depth of concrete with UPV. The cracks which were taken into this research were the surface cracks. They applied the surface probing method. This was used to measure the sonic velocity on a surface. Both transmitter and receiver are located in the same surface area. The specimens which they used in their study were beam-shaped specimens with dimensions of 15x15x60 cm and their compressive strength was 19 MPa. Specimens had crack depth of 2, 4 and 6 cm. For each crack depth, 3 samples were made. Also, the reinforcement was placed in the middle at the depth of 4 cm. The diameter of the reinforcement was 8 mm. The scheme of the measurements is shown in Figure 12 (Baehaki et al., 2019).

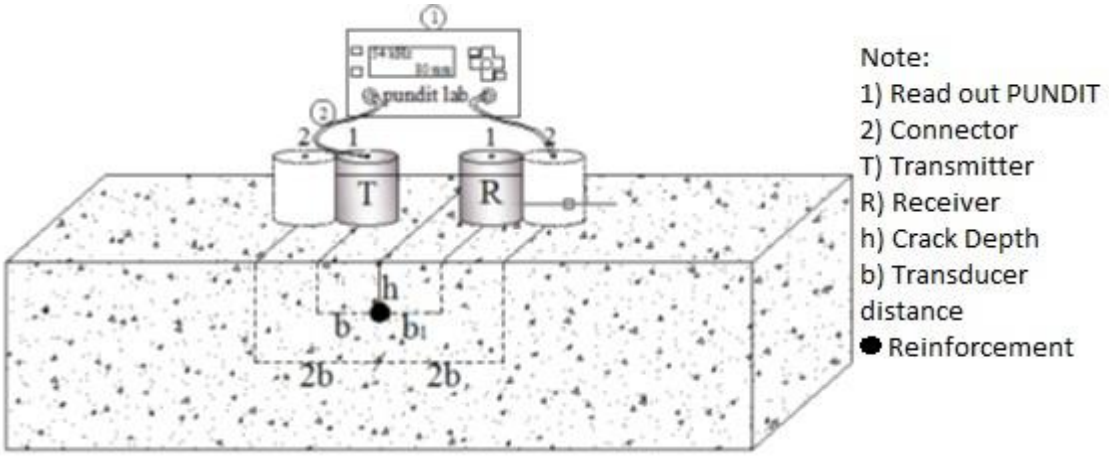

Figure 12: Concrete Crack Depth Testing scheme (Baehaki et al., 2019)

The conclusion was that the sonic velocity was affected by the distance between transducers. Also, the reinforcement influenced the test results. Samples which had a crack depth of 2 cm had a relative error of 36.8%. The samples which had a crack depth of 4 cm had a relative error of 16.5%. The test object with a 6 cm crack depth has a smaller reading result with a relative error of 3.4%. In addition, it obtained an effective transducer distance of 12 cm with an accuracy of 85.4% (Baehaki et al., 2019). This means that the greater accuracy of the measurement is achieved when the crack depth is greater and also when the distance between the transducers is greater.

3.1.3 Setup

For acoustic wave generation, the electric signal should be applied to piezoelectric element. The acoustic setup consists of following components:

- Function generator,
- Amplifier,
- Piezoelectric elements (these may work as transmitter and receiver) and,
- Oscilloscope.

Function generator is built within the oscilloscope. It is run with the Pico Scope software on the computer, which is connected to the oscilloscope via USB. Oscilloscope collects the waveforms and generates them in the software. The amplifier is connected to one channel and amplifies the voltage for the piezoelectric element which works as a transmitter. The transmitter is connected to the amplifier and it will be set on the object where the transmission of the ultrasonic waves is desired. The coupling of the piezoelectric elements to the object (in this case, autoclave) is also very important. The coupling can be done with the cable tie or a high-temperature resistant tape. In order to reduce noise in the signal, ultrasonic gel is applied to all piezoelectric elements.

Figure 13 shows the ultrasonic setup. In this case, 2 piezo elements are connected to the cement sample with a tape. The green element works as a transmitter, and the blue one as a receiver. The receiver is connected to the oscilloscope with the channel A, and this will show the receiving waveform. The transmitter is connected to the amplifier (, and this is connected to the oscilloscope via channel B. In this case, channel B would be a visual presentation of the transmitter waveform and channel A is the receiver waveform. As mentioned before, the oscilloscope is connected to the computer with the USB cable to the computer. In case the third piezo element would be used, it may be connected to either channel C or D. In any case, you may connect any element to the oscilloscope to any channel but be aware what is the function of each of them.

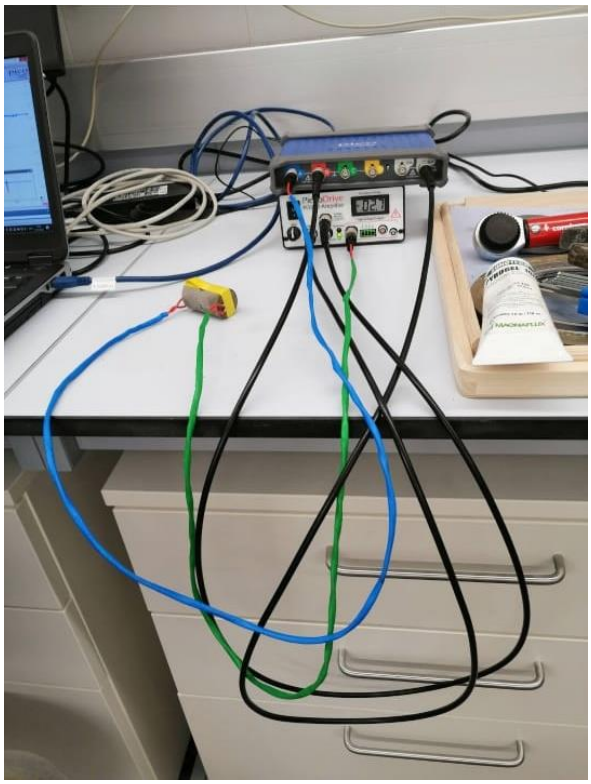

Figure 13: Ultrasonic setup in the lab

Figure 14 shows a scheme of the experimental setup for acoustic measurement together with the autoclave. In order to fix the piezoelements properly, a tape and an ultrasonic coupling gel is necessary. The tape has to be resistant to high temperature. The measurement of the travel time occurs by setting up a receiver opposite to the transmitter. Also, the travel time needs to be calibrated. This is done by deducing travel time of other materials in the autoclave. After deduction, only travel time of the cement remains unknown, which is gained by the measurement. The other receiver's position is below the transmitter. This receiver collects reflections. Cement damage changes the reflection of waves. Some properties of the material correlate with the travel time of the ultrasonic waves. One such property in the cement is its compressive strength. The compressive strength of the fresh cement increases as the cement sets. As the cement sets, compressive strength increases. This causes deduction of the travel time. Greater connection of cement molecules result to a better propagation of the sonic waves (Wagner, 2020).

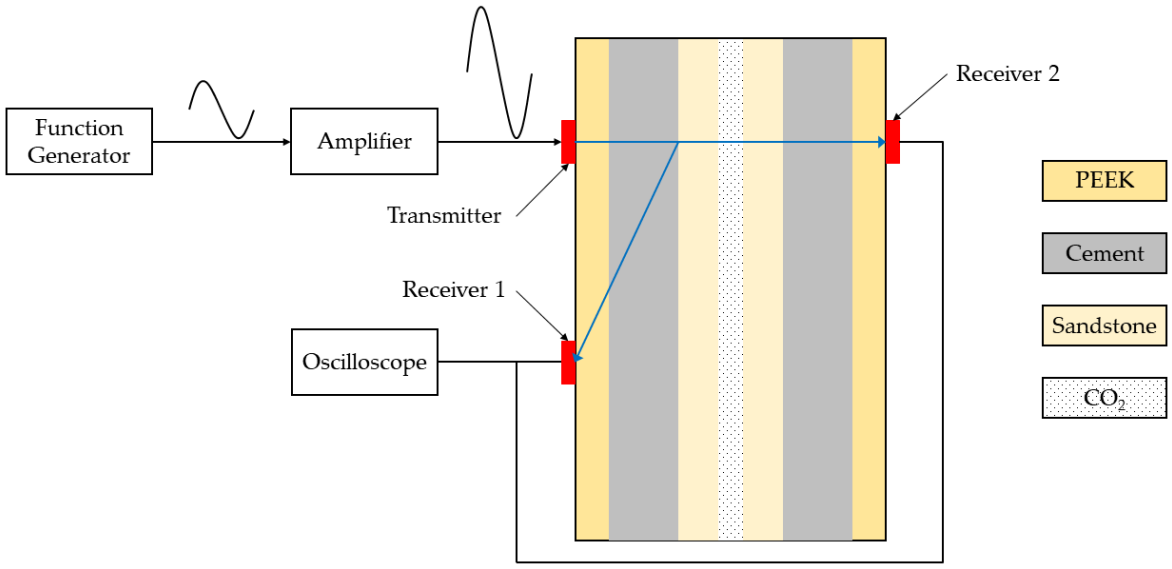

Figure 14: Ultrasonic system for the autoclave (Wagner, 2020)

For acoustic measurement in the Pico Scope software, rulers have to be used in order to make measurements. Measurement example is demonstrated Figure 15.

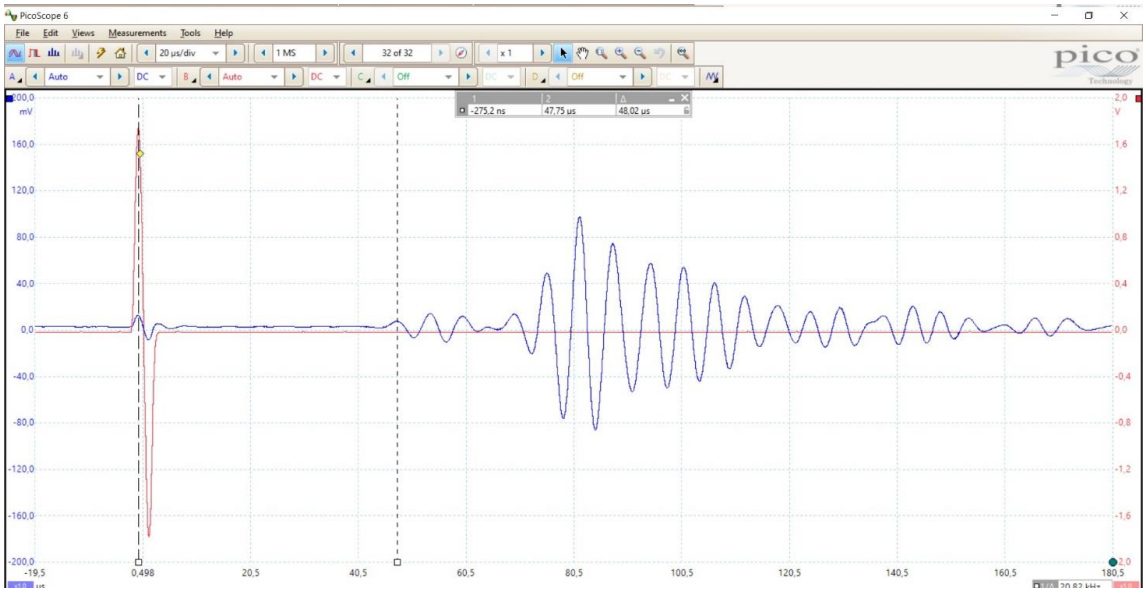

Figure 15: Example of measurement in the Pico Scope software

In the bottom left corner in Figure 15, the ruler appears in a form of square and it needs to be dragged and dropped to establish the starting point of the measurement. Then another square will appear on the same spot and it may be used to mark the end point. The difference between them will show you the difference in time between them. In the upper left corner, the same principle works, but in this case, it will measure the difference in voltage. Same thing works for the red square in the upper right corner, but this shows the voltage in the different channel. White squares and their lines measure the time. The reference points which have to be taken for the measurements are the first peak of the transmitter sine wave (red line), and the first peak of the receiving signal after the

relaxation period (blue line). This means that the acoustic waveform from the transmitter arrived.

The waveform which was selected for the acoustic measurement is the sine wave which consists of the following:

- A sine wave which has a frequency of 200 kHz and it pulses every millisecond and,
- a silence period between two pulses.

The purpose of the silence period is that the receiving piezoelectric element has enough time to gather the ultrasonic waves from the transmitter. In normal sine waveforms, that would be impossible because there is no silence period which allows for the receiving piezoelectric element to receive the acoustic wave from the transmitter. The recommendation is to make the same measurement multiple times to confirm the repeatability and the accuracy of the measurements. Sonic velocity needs to be calculated by dividing the length of the pathway the signal needed to go through with the time it took to arrive to the receiving piezoelectric element.

3.2 CT Scanning Method

The computer tomography (CT) scanning is a nondestructive technique applied to analyze the internal microstructure of materials based on the intensity of the X-rays which go through the material. CT equipment has two fundamental parts. The first one is the emitter. It emits the rays at an intensity which is predefined. The second important part is the detector. This registers the reception intensity of the emitted rays. During the analysis, the object rotates in front of the scanner. The emitter emits rays in all directions of the plane. After the intensity of the rays at the detector is being processed, an image may be created. This image may be useful to determine the density of the objects within the recorded image. The process is then repeated for different sides of the specimen. This repetition results in a 3D information of the specimen. Alternatively, a conic beam of X-rays will be emitted that are collected on a flat detector. Only the rotation of the specimen is necessary in this case. The resulting image is in greyscale. The intensity of the gray color matches the density of the specimen at that point. Where the density is lighter, the darker the color is. Also, the heavier density is represented with a lighter gray color. This technique started for medical purposes. In the recent years, this technique was also used for other scientific purposes. Science and engineering are especially using it, where all variants of computerized tomography are increasingly employed (Vicente et al., 2017).

To give a clear example of how the CT scan is applied for the carbonation analysis, the work of Paul Wagner is going to be used. For one experiment, the cement slurry with the density of 1.38 specific gravity or 11.5 pounds per gallon (ppg) is poured into the autoclave and it was let set. After that, the initial scan before the injection of carbon dioxide was made. Multiple scans were performed until the experiment got terminated. The comparison between the initial and final image of the side cross-sectional view is shown in Figure 16. (Wagner, 2020)

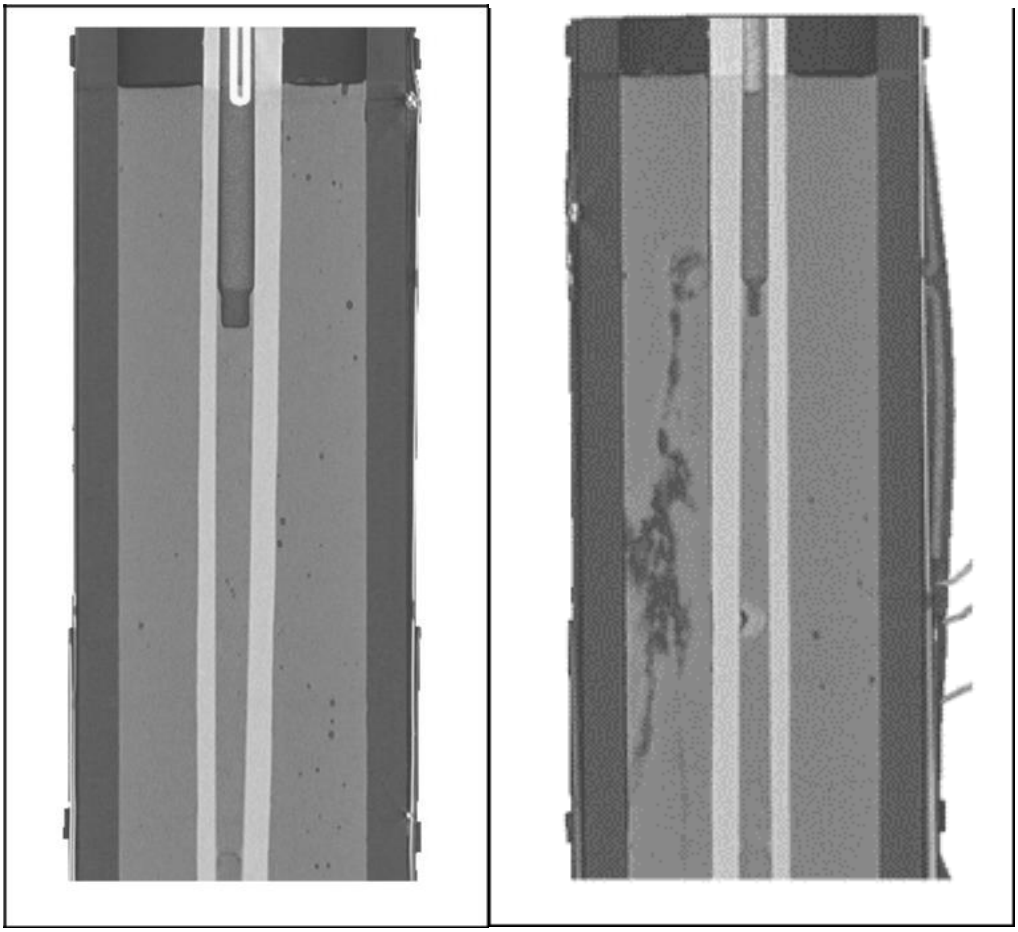

Figure 16: Comparison of the side cross-section view before and after carbonation (Wagner, 2020)

From this Figure, the difference is visible. As you can see, on the right image, a crack got developed, which is shown in darker gray image. As mentioned before, the darker the gray color, the less the density it is.

3.3 Destructive Test Methods

The uniaxial compressive strength is generally a measure of the strength of a material. This is also the maximum axial compressive stress that a sample of a material can withstand before failing. It is also known as unconfined compressive strength because confining stress is set to zero (Schlumberger Oilfield Glossary, 2021). This testing method uses either cubic or cylindrical specimen. For the purpose of this thesis and for other testing of the cement properties, the cylindrical molds are going to be created.

By the ISRM standard, specimen has to be in a circular shape. The height to diameter ratio has to be between 2 and 3. Also, the ends of specimen need to be flat in order to have the best accuracy in the measurement of the uniaxial compressive strength. The elastic modulus is basically unaffected by the specimen size. For the larger specimens, the compressive strength and the brittleness are reduced. Also, the larger the specimen, the greater number of micro cracks could occur within the specimen, which will increase

the probability of a more severe flaw. Regarding the shape of the specimen, the elastic modulus is unaffected by it. As the aspect ratio increases (the height to diameter ratio), the strength and the ductility of the material decrease. For this reason, the best height-to-diameter ratio to use for the specimen preparation is 2. In case other height-to-diameter ratio is used, the coefficient needs to be applied to calculate the correct uniaxial compressive strength. The chart for it is visible in Figure 17. (Pittino, 2020)

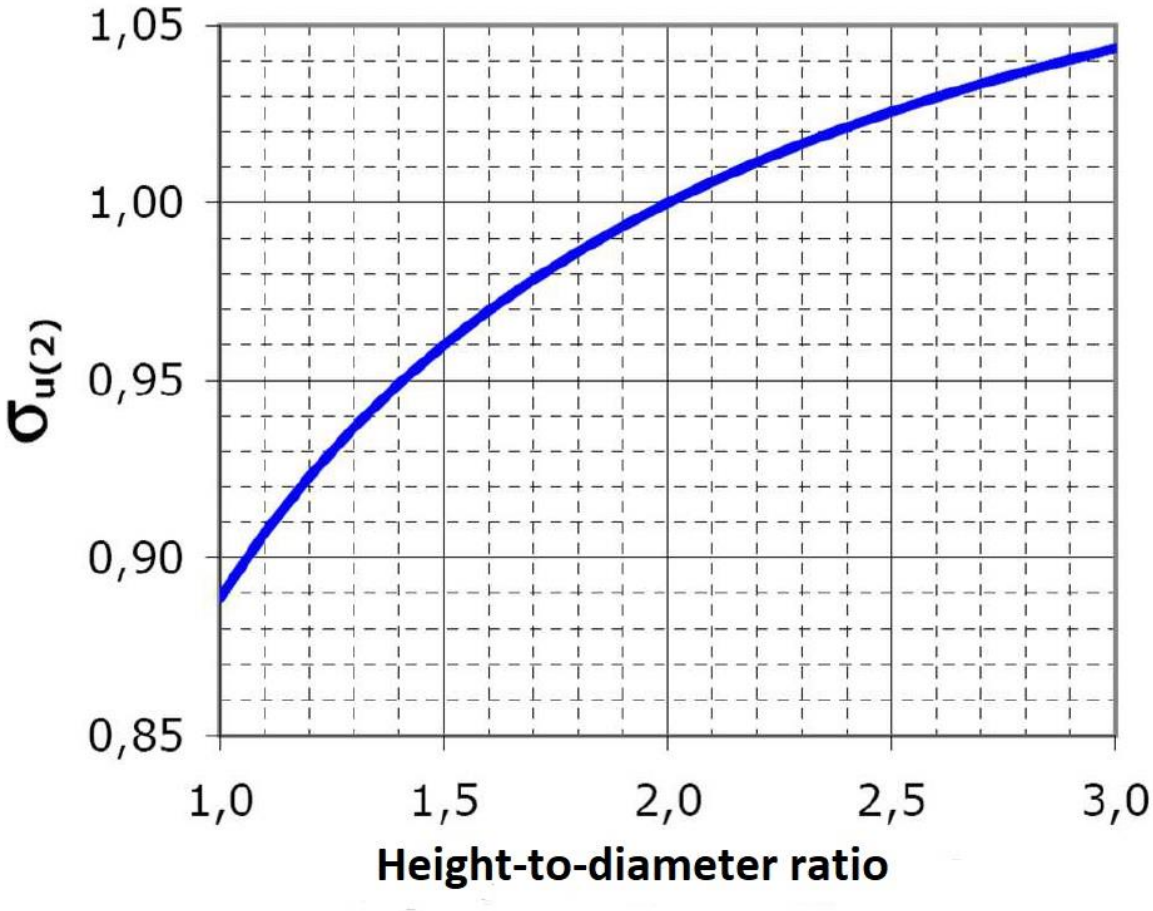

Figure 17: The correction factor applied to different height-to-diameter ratios (Pittino, 2020)

This can be mathematically expressed with the Equation 20 (Pittino, 2020).

$$\sigma_{(2)} = \frac{8*\sigma}{7+2\frac{d}{l}} \tag{20}$$

Where:

- $\sigma_{(2)}$ is the compressive strength when the height-to-diameter ratio is 2 [MPa],
- σ is the recorded compressive strength [MPa],
- d is the diameter of the specimen [mm] and,
- l is the length of the specimen [mm].

The Brazilian Test is a laboratory test to determine the tensile strength of rocks. As the tensile strength is much lower compared to the compressive strength, it is a very important parameter. This parameter contributes to the design of a geotechnical project.

This is also a characteristic of concrete. Due to low tensile strength, the steel reinforcement was introduced. This improved the tensile strength of the material. During compression, the tensile strength in the tips of the micro cracks is exceeded and they tend to propagate through the specimen until the specimen fails. Direct Tensile Strength (DTS) is the most valid method to find the true tensile strengths, but the preparation of the specimens for that test is usually time consuming and difficult. As the specimen should fail in the middle, the Direct Tensile Strength test method is not reliable. Therefore, a switch to indirect tensile strength testing is desired. One example of an indirect tensile strength test method is the Brazilian Tensile Strength (BTS) test. For this test, the specimen which is prepared is in cylindrical shape and its thickness should optimally be equal to half of the specimen's diameter (Geoengineer, 2021).

Sample is set between two jaws which are assembled together. This is made because they can make contact with the sample in the opposite ends. The upper jaw contains a spherical opening where a circular half-ball bearing is placed. Test configuration os demonstrated in Figure 18. (Geoengineer, 2021)

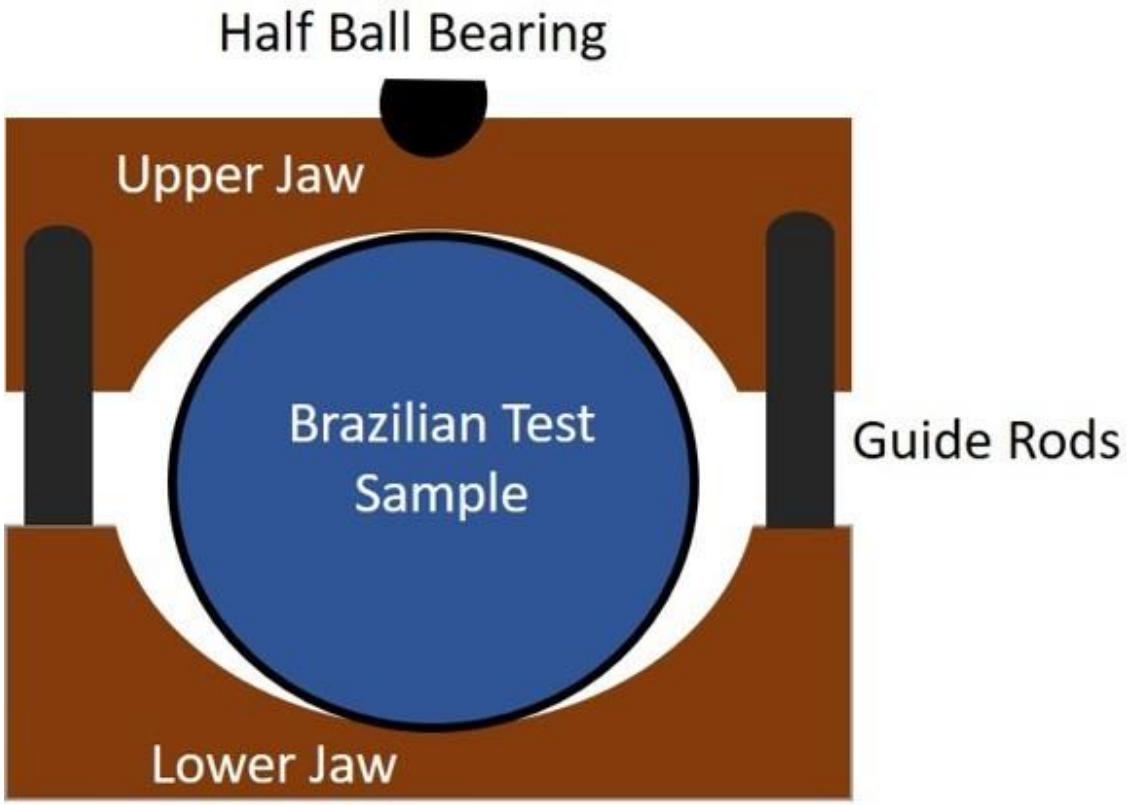

Figure 18: Brazilian Test configuration (Geoengineer, 2021)

The system together with the sample is set in the loading apparatus. The loading apparatus gives a constant load rate. In this way, the sample will fail between 15 and 30 second. The maximum load is then recorded. Sample has to fail along its diameter. In case it does, the test is valid. The formula to calculate the tensile strength of the specimen is in the Equation 21.

$$\sigma_t = \frac{2*d}{\pi*d*w} \tag{21}$$

Where:

- σ_t is the sample tensile strength [MPa],
- P is the maximum load [N],,
- w is the sample width [mm].

The XRD and SEM are the testing methods with which the chemical analysis is going to be performed. With it, the chemicals which are present in the carbonated area may be discovered. Also, based on these two methods, the mineralogical analysis may be performed. Figure 19 shows a comparison of two SEM pictures (Jobard et al., 2018).

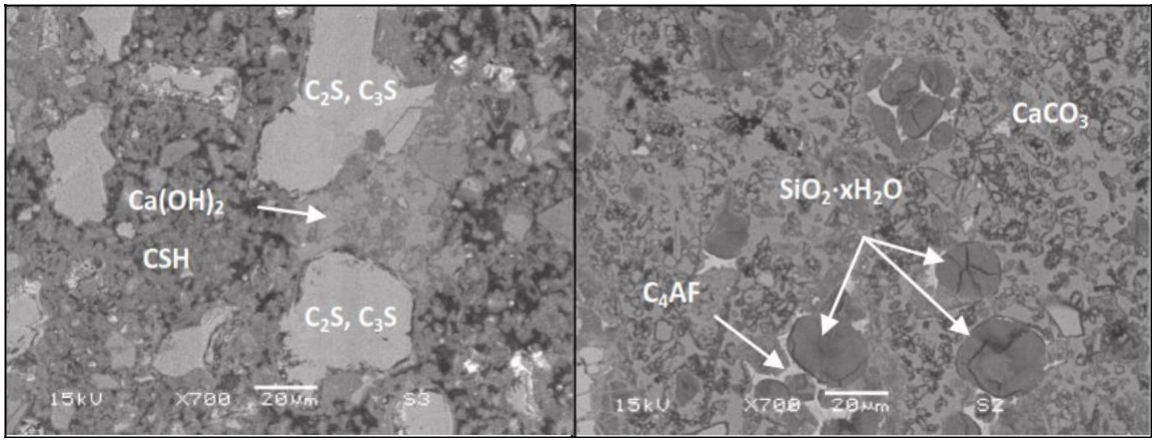

Figure 19: Comparison of two SEM pictures taken before (left) and after carbonation (right) (Jobard et al., 2018)

The picture on the left demonstrates the cement before carbonation occurs. This cement contains the common cement phases of calcium hydroxide, calcium silicates, and C-S-H-phases. The right picture shows the situation after the cement gets carbonated. It leads to the genesis of calcium carbonate and silica gel. The round beads which are marked with SiO_2*xH_2O, are amorphous silica gel. The pictures demonstrate the alteration of chemical composition of the cement after carbonation. Figure 20 demonstrates another SEM study (Jobard et al., 2018).

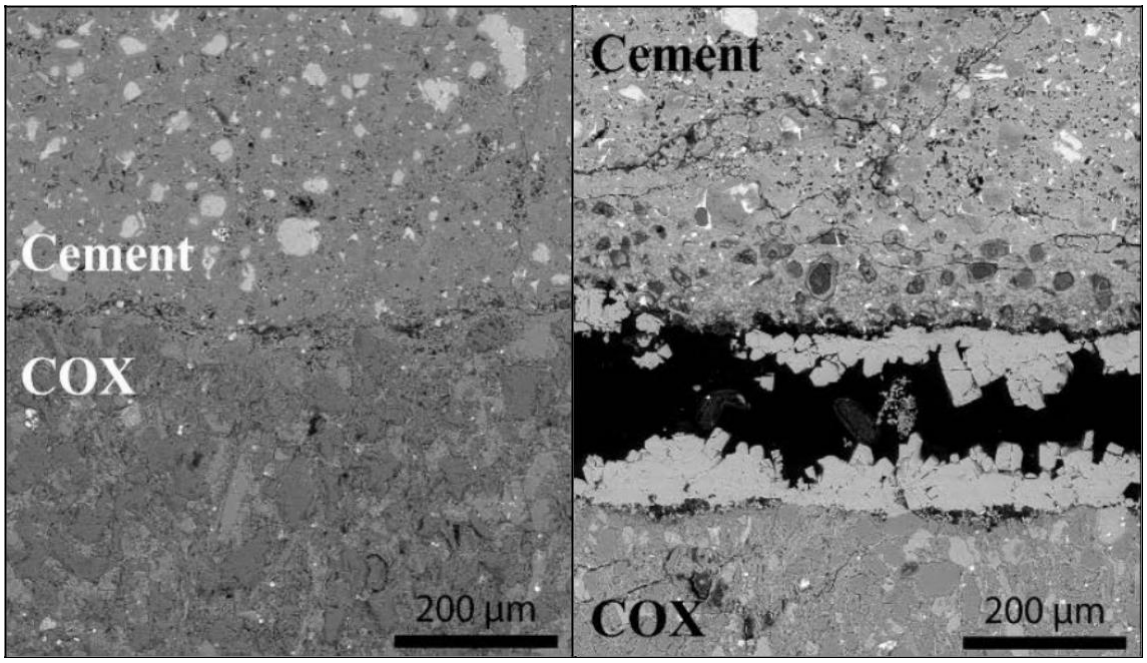

Figure 20: SEM pictures of cement-rock interface after the exposure in nitrogen (left) and carbon dioxide in solution (right) (Jobard et al., 2018)

Sample preparation was made with putting a rock sample into a mold made by silicon. The cement slurry was poured around the mold. The exposure of carbon dioxide happened in various conditions. The nitrogen atmosphere was taken as a reference in this study. The left picture shows no change in bond between the cement and the rock. The right picture demonstrates the same setup in carbon dioxide. In this case, the bond between the rock and cement deteriorated. Calcium carbonate crystals were also generated in these conditions (Jobard et al., 2018).

Chapter 4 Experimental Process

4.1 Previous Research on Carbonation

Jobard et al. studied the effect of supercritical carbon dioxide on an interface between clay rock and Portland cement. The slurry preparation happened according to API RP-10B-2. For their sample preparation, they placed a 25x17x10 mm hydrated cap rock sample in the middle of a 35x30x20 mm silicone mold. After 24 h of setting, they removed the silicone. After the setting period, they placed the samples in a reactor filled with a natrium chloride solution. The conditions within the reactor were the pressure of 100 bar and a temperature of 80°C. After seven days, the first sample was removed. Eight samples were cured in a period of up to 30 days in various conditions. Whenever the sample was removed, a depressurization of the reactor happened. Their findings included alterations mechanisms, like carbonate precipitation, cracking of the cement, and leaching of calcium-bearing phases. They also found that supercritical carbon dioxide leads to much stronger carbonations (Jobard et al., 2018.).

Aiex et al. conducted an intermediate step within the carbonation process. They submerged the samples in carbonic acid. Pressure is applied with carbon dioxide onto the carbonic acid bath. The conditions inside the chamber were 137.9 bar and 73.9 °C. There were various types of samples, like different cement classes and a wide range of additives. Time of sample exposure went to a maximum of one year. Chamber was depressurized in order to withdraw samples for analysis. Portland cement with freshwater gave the best results in terms of compressive strength after exposure (Aiex et al., 2015).

Lacerda et al. wanted to document the front of the cement carbonation. It was conducted by using pH-probes and micro-CT scans. The prepared cement was a high strength Portland cement. It was also mixed with sand in a 1:3 ratio. They prepared 11 cylinder specimens with a diameter of 2 cm and a length of 4 cm. Lacerda et al. determined the baseline with one specimen, and the remaining 10 went into the curing chamber. The samples were not exposed with supercritical carbon dioxide. They were in a curing tank with 5% carbon dioxide, humidity of 65% and a temperature of 28°C. Samples were removed after 25 days and pH and micro-CT analysis was conducted. For carbonation front visualization, phenolphthalein was applied. It was concluded that the indicator was not able to provide information on the carbonation of the innermost region. For a greater understanding of carbonation, pH-values and binarized micro-CT scans made a great contribution to it (Lacerda et al., 2017).

Wagner constructed an autoclave in order to get real-time monitoring of cement slurry carbonation affected by carbon dioxide. The novelty of the setup which he did lies in the fact that he was able to monitor cement carbonation in real-time without disturbing the sample inside. The autoclave was designed to withstand the pressure of 100 bar and temperature of 120°C. The pipe body was constructed with PEEK, because it enables to run the CT scan. Metals are usually magnetic and for that reason the CT scan would be impossible to make it with that material. Scheme of the pipe body is shown in Figure 21. (Wagner, 2020)

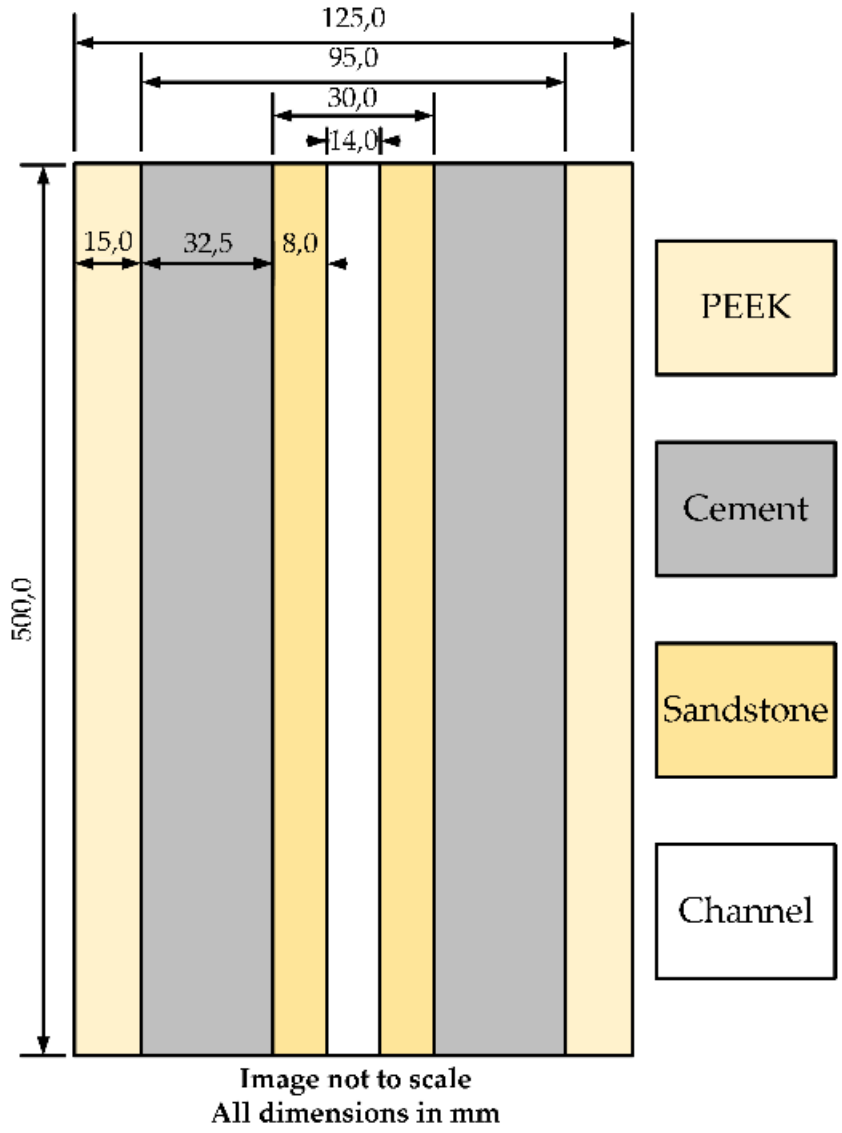

Figure 21: Schematic of the experiment sample in the autoclave (Wagner, 2020)

There were 2 experiments conducted. One was served as a heavy carbonation baseline, and the other as a light carbonation baseline. The heavy carbonation baseline experiment was conducted with the Portland Class G cement, where the only additive was bentonite. Slurry had a specific gravity of 1.38 (11.5 ppg). The cement was prepared according to API-RP 10B-2. To prepare the autoclave, it was vacuumed in order to have initial pressure close to zero and that there will be no air in the autoclave, which could affect the results of the experiment. Pressure was built up to 50 bar and the temperature was built up to around 35 °C. Continuous monitoring occurred for 162 hours and the carbonation of the cement started right after carbon dioxide injection, which made it impossible to maintain supercritical conditions in the autoclave. Measurements with the acoustic system and the ultrasonic cement analyzer (UCA) showed that the compressive

strength of the cement was significantly lower than before the experiment. The pressure started to decline due to the reaction and cement fractured when carbon dioxide was injected. The cement sheath lost integrity when it was pressurized. Fractures created flow paths for all media (Wagner, 2020).

The second experiment occurred with the Portland Class G cement with no additives, but this time the specific gravity of the slurry was 2.02 (17 ppg). Same procedure occurred as in the first experiment. After slurry preparation and installation in the autoclave, the autoclave got vacuumed to reduce the initial pressure to 0 bar. This was followed by the injection of carbon dioxide in it. The pressure got built up at around 51 bar, while the temperature built up to 50 °C. Monitoring also lasted 162 hours, but the supercritical conditions could not be achieved as it requires greater pressure. In the end, some carbonation occurred as expected around the sandstone, but the integrity of the bond stayed intact. No visible changes occurred in the cell as it was seen in the CT scan readings. The carbonation caused a decrease of compressive strength by 21%. This decrease has an impact of the integrity of the cement, but the remaining compressive strength was still high after the experiment. The bond between cement and sandstone showed that the integrity of cement stood intact (Wagner, 2020).

4.2 Design of the Autoclave

This section dedicated to the autoclave design for experimental purposes. Initial design was made by Paul Wagner, which was then modified to the current design of the autoclave. Also, future design will be briefly discussed with the complete system.

4.2.1 Initial Design

As mentioned before, the material selection requirement for the autoclave body was the ability to use it in a medical CT-scanner. Prior to this, no method for continuous carbonation monitoring existed. Therefore, CT-scans also helped to develop other monitoring measurements. The issue here is that autoclaves usually are made of steel or other metals, which render a CT-scan of the inside impossible. Because of that, the PEEK was chosen as the material for the autoclave body. The configuration of the autoclave, as mentioned before, permitted a maximum pressure of 100 bar and a maximum temperature of 120°C. PEEK allowed a maximum temperature of 350°C and sealing parts set the maximum pressure. Figure 22 shows the plan of the initial autoclave design. It is shown in a form of exploded view (Wagner, 2020).

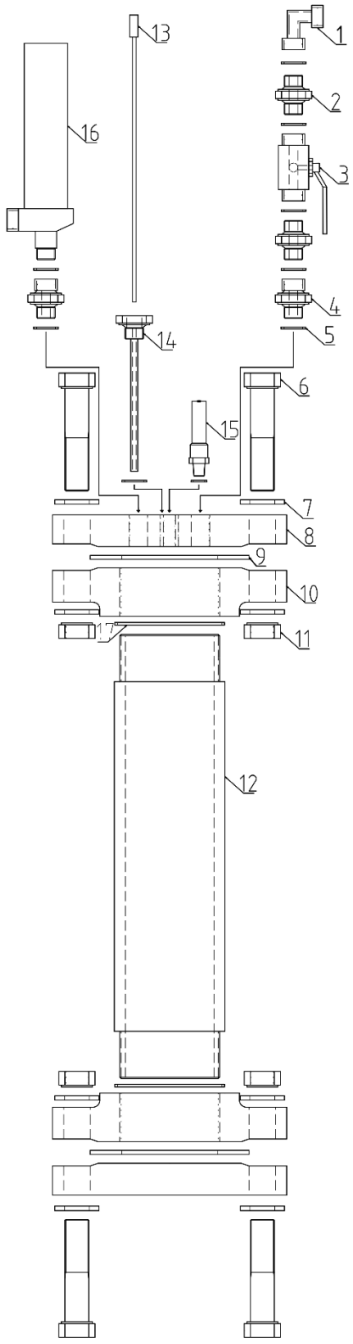

1. 90° fitting, female connectors on both ends
2. Straight fitting with male connectors
3. Two-way valve
4. Straight fitting with a male and a female connector
5. Gasket
6. M27x115 bolt
7. M27 washer
8. Top flange with three G ½" female connectors and one NPT ¼" female connector made from type 5 DN 100 PN 100 flange
9. Graphite sealing element
10. Type 13 DN 100 PN 100 threaded flange
11. M27 nut
12. PEEK pipe body
13. Thermocouple
14. Thermowell
15. Pressure transducer
16. Safety valve
17. O-ring seal

Figure 22: Exploded view of the initial autoclave design (Wagner, 2020)

Flanges which were used for the autoclave are defined by the EN 10226-1 standard. PEEK is designed in a pipe form. Cutting this pipe to the desired length of 50 cm and threading it delivers the necessary pipe. The seal which proved to be gas tight was an O-ring with a groove in the pipe. Assembly and disassembly is easy with this design. Standard gaskets are applied as the sealing element. In order to reuse the elements,

inspection is needed. This is also applied for sealing surfaces. Closing the flanges must be carried out by a trained person (Wagner, 2020).

The construction of the initial autoclave occurred under the goal to reuse every part in every experiment. No waste parts were present as there is no bond between the cement and PEEK (Wagner, 2020).

4.2.2 Current Design and Future Design

The current design is based on the initial design made by Paul Wagner. The PEEK body is cut in this case to 30 cm. With it, the sandstone length got cut shorter as well. Due to fittings and elastomers which are going into the autoclave itself, the length of sandstone is shorter than the PEEK pipe body. Currently the sandstone core is 26.5 cm long. Also, the top of cement is above the top sandstone to ensure the carbon dioxide will not go into empty space straight after cement failure and redirect the flow through that space. The innovation for this design is the introduction of dynamic testing system, which will occur in the moment the cement fails. Dynamic testing starts in the moment when the manometer measures pressure in the outlet above zero. Figure 23 shows the updated design.

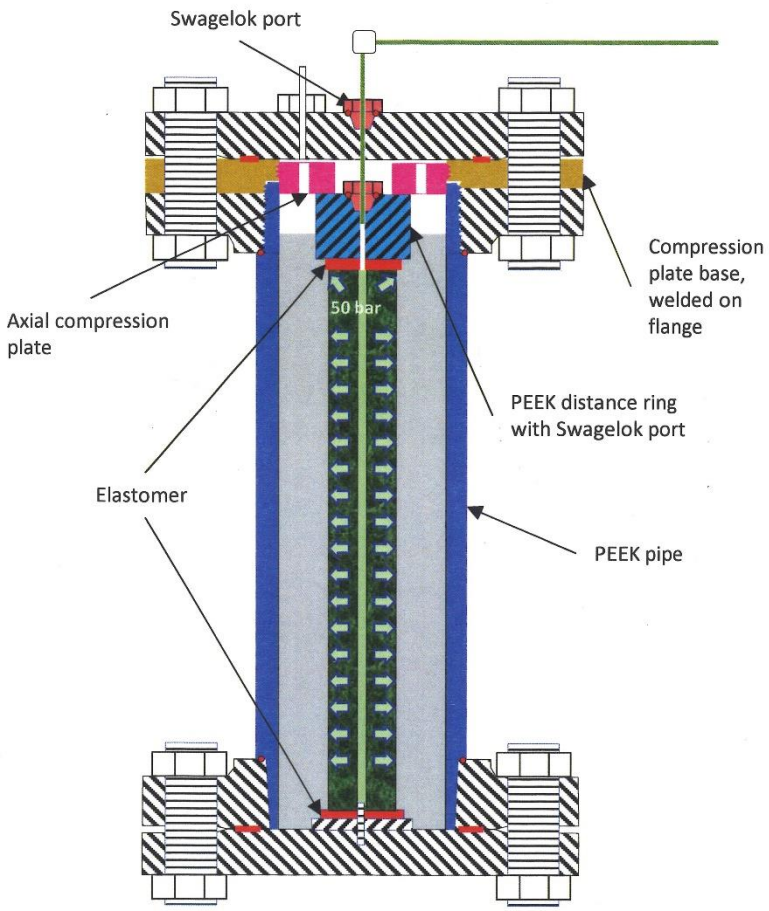

Figure 23: Current design

In the future, pumping system is going to be introduced. The purpose of it is to maintain the pressure within the autoclave above the critical pressure of carbon dioxide. With the current design, the weight of the autoclave got slightly reduced, but future design considerations are also focused on the way to optimize the weight of the autoclave. For the initial and current design, there are always at least two people necessary in order to transport the autoclave to places where the experiment will be conducted, the CT scan will be performed etc.

4.3 Experimental Apparatus and Procedure

4.3.1 Experimental Apparatus

Multiple devices are necessary in order to conduct the experiment properly. Also, there will be experiments done in parallel to the carbon dioxide injection in order to determine the cement properties. Devices are located in the laboratory of the Chair of Drilling and Completion Engineering in the Mining University of Leoben in Austria.

Mass of required materials, including class G cement, bentonite, barite, and water were measured with the FCB 3K0.1 electronic scale, manufactured by Kern. The weighing

capacity and readability of the scale were 3.0 kg and 0.1 g, respectively. According to the API RP 10B-2 standard, the accuracy of the scale should be within ± 0.1% that the scale meets it. Figure 24 shows the electric scale.

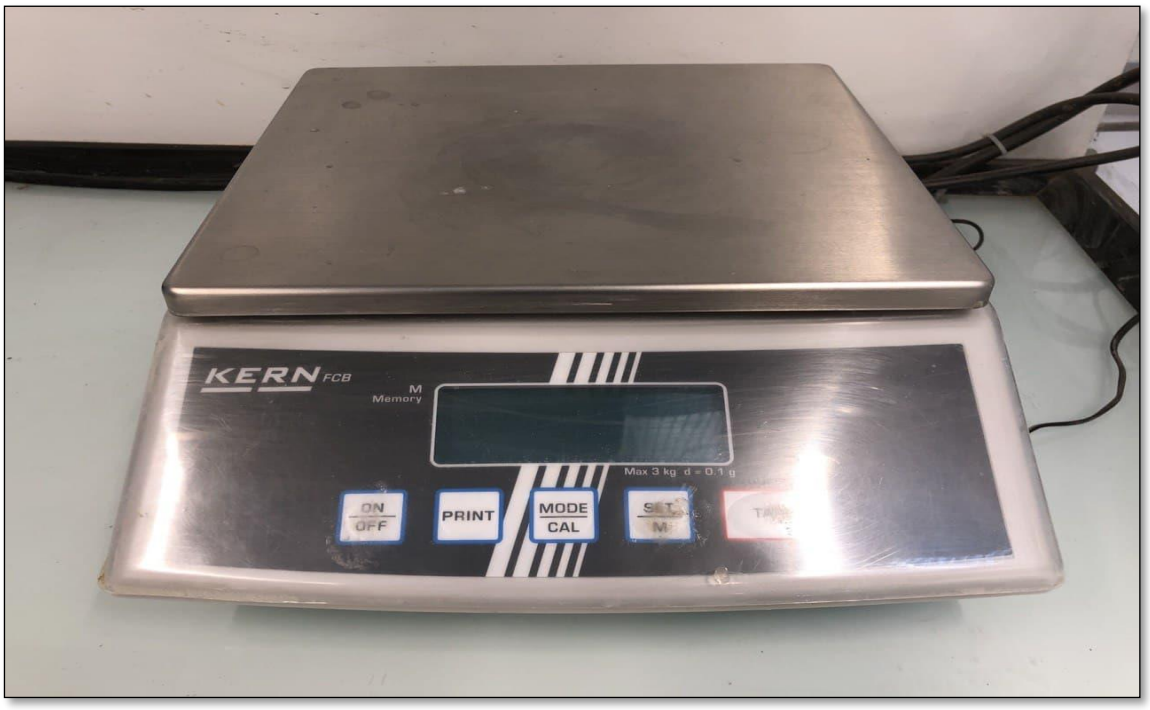

Figure 24: Electric Scale

For the experiments which determine the composition which is going to be used for the actual experiment, Chandler engineering's constant speed mixer model 3260 with a one-liter cup was used. The built-in mixer program was set for the speed of 4,000 ± 200 RPM for 15 seconds. During that time, the cement with additives needs to be uniformly mixed with water. After that, the speed increases to 12,000 ± 500 RPM according to API specification 10. The mixer is also able to provide and manually set a constant mixing speed from 1,000 to 20,000 RPM (Chandler Engineering Company, 2015, a). Also, for the slurry with prehydrated bentonite, the bentonite is mixed with water at the speed of 4,000 ± 200 RPM for a minute to make sure the bentonite is mixed with water properly for prehydration process. The mixer is shown in Figure 25.

Figure 25: Chandler Constant Speed Mixer Model 3260

In order to mix a large volume of the slurry, which is going to be needed for the experiments, a batch mixer with the stainless steel container is used. The batch mixer has three RPM settings: 197, 317 and 462 RPM. The mixing procedure for the batch mixer consist of adding the liquid components into the container while mixing at 197 RPM and setting the speed to 462 RPM afterward. Uniform addition of components makes sure that the distribution will be even within the stirred liquid. For a proper slurry, ingredients should be mixed for 10 minutes (Wagner, 2020). For the prehydrated bentonite cement slurry, the idea is to mix the bentonite with water at 197 RPM for two minutes to make sure the bentonite is uniformly distributed to the mixture. After that, the mixture has to be static for at least 30 minutes to make sure the prehydration process is complete. Figure 26 shows the batch mixer with the stainless steel container.

Figure 26: Batch mixer with the stainless steel container

For the cement slurry, which was mixed in the Chandler Constant Speed Mixer, the Atmospheric Consistometer Model 1200 was used to make sure the air bubbles are not in the slurry anymore and the mixture is consistent. Slurry conditioning in atmospheric pressure are performed by the atmospheric consistometer. In addition, it can determine different parameters such as water content of slurry, fluid loss, and rheological properties of the slurry in compliance with API Spec 10A. It contains a stainless steel water bath that can be heater up to 93°C. It also has two slurry containers with a capacity of 28 cubic inches, where slurry is poured into (Chandler Engineering Company, 2015, b). A motor rotates the slurry containers at 150 RPM based on API Spec 10A. Figure 27 shows the applied atmospheric consistometer.

Figure 27: Atmospheric Consistometer Model 1200

As the volume of the atmospheric consistometer is limiter, an alternative was needed in order to have a consistent slurry mixture for large volumes. For this reason, a vibrating table is attached to the floor, where the process of slurry conditioning happens. The stainless steel mixing container with the slurry is fixed to the vibrating table with poles and nuts with seals. The conditioning on the vibrating table lasts for 30 minutes. Preliminary experiments showed that this duration most accurately mimics the API RP 10B-2 slurry preparation scheme (Wagner, 2020). As the vibrating table makes a lot of noise, ear protection during the conditioning process is recommended. Figure 28 shows the vibrating table together with the mixing container.

Figure 28: Vibrating table with the mixing container

In order to determine the actual density of the mixed cement slurry, the Ofite Atmospheric Mud Balance was used. The mud balance has four measurement units, which are:

- specific gravity (s.g.),
- pounds per gallon (ppg),
- pounds per cubic feet (pcf),
- and psi per 1,000 feet.

Figure 29 shows the atmospheric mud balance.

Figure 29: Ofite Atmospheric Mud Balance

For the uniaxial compressive strength testing of molds, which are created as the reference for the correlation between the sonic velocity and the compressive strength of the cement, the testing machine mode 'Quasar 200' was used. The testing machine was made by an Italian manufacturer, Galdabini. The sample was placed in the machine with a fixed plate (bottom) and a moving plate (top). This machine may apply a maximum load of 200 kN. Top plate speed is selectable. Results of the test are shown in respective plots with the associated software (Galbadini, 2021). Figure 30 shows the testing machine.

Figure 30: The 'Quasar 200' load cell

To measure the fluid loss, the Stirred Fluid Loss Cell Model 7120 by Chandler is used. The operating temperature range is between 5 and 232 °C, while the maximum cylinder pressure could go up to 13.9 MPa. There are two different variations of fluid loss testing. One variation is the low-temperature fluid loss testing which is below 88 °C, and the other variation is the high-temperature fluid loss testing which is above 88 °C. Operating sequence differentiates between these two variations. The assembly includes an impeller that is rotate at 150 RPM. In order to collect the filtrate for measurement, a graduated cylinder is applied for that purpose. Heat to the cylinder is supplied by a tubular heater around the cylinder. To apply pressure to the cylinder, a supply of compressed air, nitrogen or another inert gas is necessary. The pressure release valve is used to release cylinder pressure. For the cooling, a water jacket is built into the unit. (Chandler Engineering Company, 2016). Figure 31 shows the fluid loss cell.

Figure 31: Stirred Fluid Loss Cell

In order to measure the rheologic properties of the cement, the Chandler Model 3500 Rotational Viscometer is used. With the measurements of the shear stress at the necessary shear rates all the important rheologic properties can be measured, namely viscosity, gel strength, and the yield point. The viscometer has a standard rotor-bob configuration of R1-B1. In this configuration, the shear rate in RPM is multiplied by 1.703 to get the shear rate is s^{-1}. Steel cup is filled to the marking with stirred slurry. The slurry volume until the marking is 350 ml. The rotor is immerged to the marked depth. The motor should be then switched on and the desired speed should be selected. On the dial the shear stress value will appear for the according shear rate (Prohaska, 2020). The viscometer is shown in Figure 32.

Figure 32: Chandler Model 3500 Viscometer

In order to get the measurement of the compressive strength of the noncarbonated cement slurry, the Model 4265HT Ultrasonic Cement Analyzer made by Chandler is used. The maximum temperature which can be applied into the device is 315 °C and the maximum pressure which may be applied is 138 MPa. In order to get the relevant measurement, the pressure and temperature are going to be the same as in autoclave. To

monitor the development of the compressive strength of the slurry, the adequate software for the ultrasonic cement analyzer is going to be used. Recording system needs to be turned on to record all the values (pressure, temperature, and the compressive strength) The slurry is prepared and placed into the test cylinder which will be placed into the analyzer during the test (Chandler Engineering Company, 2018). Figure 33 shows the ultrasonic cement analyzer.

Figure 33: Ultrasonic Cement Analyzer Model 4265 HT

In order to measure thickening time of the slurry, Model 8340 pressurized consistometer made by Chandler may be used. Closure, heating, and pressurization may be achieved quickly thanks to its design. The working pressure of the consistometer is 207 MPa. The maximum operating temperature is 316°C. Hydraulic pump generates pressure. The hydraulic system is composed of valves, filters, piping, and a reservoir. Heat is supplied by an internal tubular heater with a power of 5000 W. Thermocouples measure the temperature within the cylinder. The programmable temperature controller automatically controls the rate of temperature rise (i.e., temperature gradient). The slurry container is rotated at a constant speed of 150 ± 15 rpm by a magnetic drive. The consistency of the cement slurry is recoded on a chart as Bc (Bearden units of consistency) obtained from a potentiometer installed within the pressure cylinder. The pressure is controlled using a dynamic, programmable pressure system. Strip chart is used to record temperature, pressure, and viscosity of the slurry. The Instrument Control

System is specifically designed for PC based data acquisition. Using the software, hesitation squeeze treatments can also be simulated using the programmable motor and pressure control capabilities (Chandler Engineering Company, 2015, c). Figure 34 shows the pressurized consistometer.

Figure 34: Pressurized Consistometer

For the carbon dioxide injection, the sandstone core is used. Sandstone is the standard reservoir rock which is the reason it is being selected. It has a hole in the middle, where the carbon dioxide is going to be injected. From that hole, the carbon dioxide goes through the sandstone pores and the carbon process starts once carbon dioxide is in contact with the cement area. The length of the core for this experiment is 265 mm, the outside diameter is 30 mm, and the inside diameter is 14 mm. Table 4 shows the properties of the sandstone.

Properties	Quantity
Average Effective Porosity [%]	22.3
Uniaxial Compressive Strength [MPa]	42.52
Young Modulus [GPa]	10.54

Poisson's Ratio	0.2
Horizontal Permeability [mD]	176-199
Vertical permeability [mD]	43-87
Density [g/cm^3]	1.99

Table 4: Properties of the sandstone

This sandstone is selected due to immediate availability, as the sandstone blocks are available in the lab. In case more cores are going to be needed, enough sandstone blocks are supplied in the lab for it. Figure 35 shows the sandstone core.

Figure 35: Sandstone core

In order to install the sandstone core in the autoclave properly, the core centralizer was made out of wood. It is made in a cross arrangement so that it fits to the inside diameter of the top flange of the autoclave. The core centralizer is shown in Figure 36.

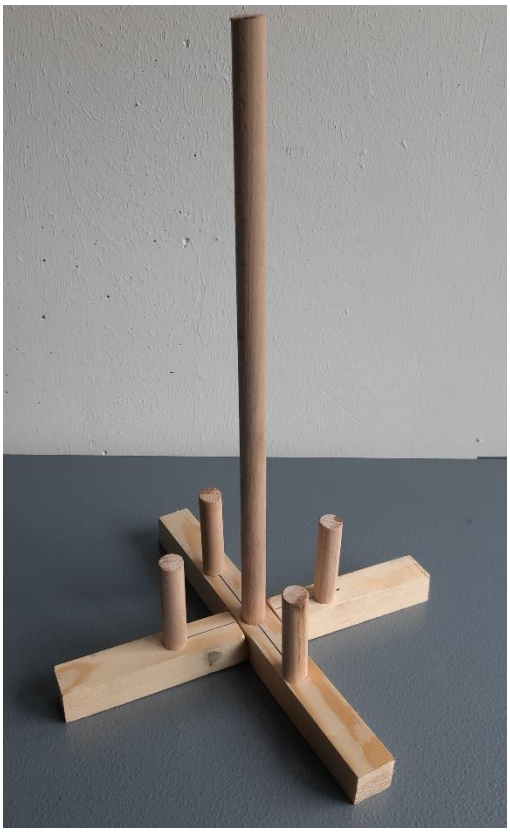

Figure 36: core centralizer

To eliminate influence on the whole experiment of any other gases than carbon dioxide, the vacuum pump is applied to bring displace the air in the autoclave with the vacuum. The process of vacuum displacement should occur before the carbon dioxide injection. Figure 37 shows the vacuum pump.

Figure 37: Vacuum pump

4.3.2 Experimental Procedure

This section shows a step by step guideline for the experimental procedure with the current design. By defining such a procedure, reproducibility is guaranteed in conducting the carbonation experiment. The procedure is divided into following steps:

- slurry mixing,
- autoclave preparation,
- slurry conditioning,
- conduction of conventional slurry tests,
- cement slurry curing in the autoclave,
- carbon dioxide injection and evaluation of cement integrity in the autoclave and,
- steps after carbon dioxide exposure.

1. Slurry Mixing
    - Mix the cement slurry in the batch mixer by adding the liquid components into the container while mixing at 197 RPM and set the speed to 462 RPM afterwards. Mixing the ingredients for 10 minutes establishes a proper slurry.

2. Autoclave Preparation
    - Place the gasket onto the bottom flange which is threaded to the PEEK pipe body.
    - Place the blind flange onto the bottom flange.
    - Make sure the gasket stays in the middle and does not interfere the placement of bolts which will seal the bottom flange.
    - Tighten the bolts together with the washer according to Figure 38. The nuts should be placed on the other side. The washer should be above the nuts.
    - Inside of the PEEK body has to be greased for easy cement removal after the experiment.
    - Mount the sandstone core using the core centralizer.
    - Fill the autoclave with cement slurry with a funnel. Move the slurry in a circular pattern for uniform placement.

Figure 38: Bolt arrangement

3. Slurry Conditioning
    - Place the autoclave on the vibrating table.
    - Condition the cement for 2 minutes.
    - Place the container on the vibrating table together with the rest of the slurry for conditioning, also for 30 minutes.

4. Conduction of Conventional Slurry Tests
    - Remove the stainless steel container from the vibrating table.
    - Measure density and rheology of the slurry.
    - Start thickening time and UCA test.
    - Start free fluid test.
    - Start stirring fluid loss test.
    - Start the sedimentation test.
    - Pour conditioned slurry into 12 cylindrical molds with 28 mm diameter and 56 mm length.
    - Evaluate stirred fluid loss.
    - Evaluate free fluid test.
    - Evaluate the UCA and thickening time test.
    - Evaluate the sedimentation test.

5. Cement Slurry Curing in the Autoclave
    - Remove the autoclave from the vibrating table.
    - Put the ultrasonic sensors to the outside of the PEEK body. Attach to it and start recording the sensor data.
    - After 2 hours of curing, extract possible free fluid.
    - After 3 days, close the top flange of the autoclave with the same procedure as the bottom flange closure.

6. Carbon Dioxide Injection and Evaluation of Cement Integrity in the Autoclave
    - Align the vacuum pump to autoclave and apply vacuum to the autoclave. By vacuuming the autoclave, the air leaves the autoclave, and no additional parameters may influence the carbonation.
    - Align the carbon dioxide bottle and apply the 50 bar pressure.
    - Attach the heating jacket using the temperature resistant zip ties.
    - Heat the cell to 50 °C to achieve the supercritical temperature for carbon dioxide.
    - Monitor pressure, temperature, and ultrasonic readings.
    - Conduct first CT scan.
    - Conduct CT scans according to carbonation speed.
    - After the degree of carbonation is sufficient, the experiment comes to an end.

7. Steps After the Carbon Dioxide Exposure
    - Release the pressure. The pressure release rate should be maximum 1 bar per minute.
    - Loosen top flange.
    - Remove cement from PEEK pipe.
    - Remove the core from PEEK pipe.
    - Drill 12 25.4 mm (1″) diameter and 50.8 mm (2″) long cores from the cement sheath. These cores are used for mechanical analysis.

4.4 Risk Assessment

Legal basis has to be determined in order to identify and evaluate the risks within the experimental process. This is conducted by the pressure equipment monitoring regulation (in German: Druckgeräteüberwachungsverordnung, DGÜW-V) in Austria. The pressure containment product is an index which is a product of multiplication of pressure in bar and volume in liter. In case of low-risk equipment, operator takes care of the risk assessment. In the other case, a testing procedure has to be approved by the government (Österreichische Bundesverfassung 2004). The scheme for the distinction between low- and high-risk pressure equipment is shown in Figure 39.

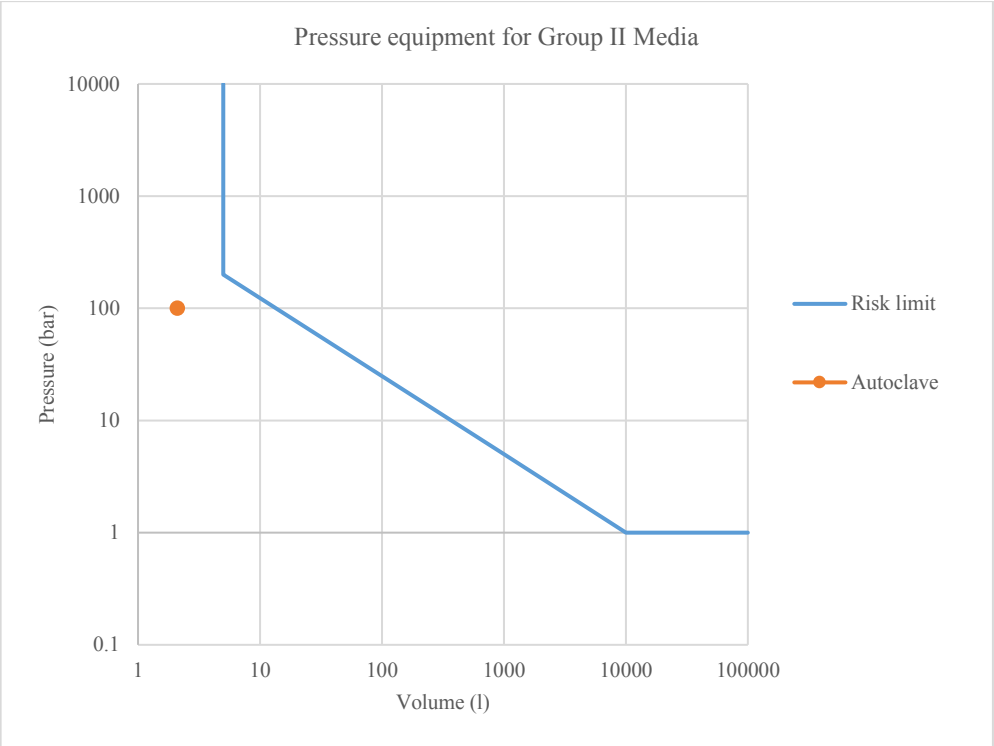

Figure 39: A scheme showing the difference between low and high-risk equipment which contains media of group II

The media within the equipment is divided into group I and II. Media of group I pose serious safety hazards. Media of group II do not contain such a hazard compared to media of group I. Carbon dioxide in this case belongs to group II. (Österreichische Bundesverfassung 2004).

Once the medium is known along with size and maximum allowed pressure, the classification may be established. Autoclave has a maximum pressure of 100 bar. It has also a total volume of 3.93 liters. This makes the pressure containment product of 393. When the equipment contains a medium of group II, it may pose a threat if:

- a maximum allowed pressure greater than one bar,
- a volume greater than 5 liters and,
- a pressure containment product greater than 1000.

As the autoclave and the medium do not go above the limit, this means that the equipment possesses a low risk (Österreichische Bundesverfassung 2004). Table 5 shows all risks within the experimental procedure. All risks are assigned with a likelihood and severity which are used to place the risks into a matrix. Figure 40 shows the matrix used for the evaluation. High-, upper-, and mid-risks require mitigation. After mitigation, all risks should be classified as low.

Procedure phase	Risk No.	Task	Risk	Likelihood [1-5]	Severity [1-5]	Classification [1-25]
1	1.1	Slurry mixing	Loose hair or clothing caught in the stirrer	3	4	12
1	1.2	Slurry conditioning	Stainless steel container or autoclave dropping off the vibrating table	2	3	6
3	3.1	Autoclave assembling	Dropping heavy objects	2	3	6
3	3.2	Attaching ultrasonic sensors	Electrification	2	3	6
3	3.3	Injecting carbon dioxide	Burst of the autoclave	1	5	5
3	3.4	Injecting carbon dioxide	Carbon dioxide leak	2	1	2
3	3.5	Heating the autoclave	Burst of the autoclave	1	5	5
4	4.1	Conducting CT scans	Dropping heavy objects	2	3	6
5	5.1	Relieving pressure	Carbon dioxide emission	5	1	5
5	5.2	Loosening flanges	Dropping heavy objects	2	3	6
5	5.3	Removing cement and rock core	Dropping heavy objects	2	3	6

Table 5: Risk evaluation for experimental process

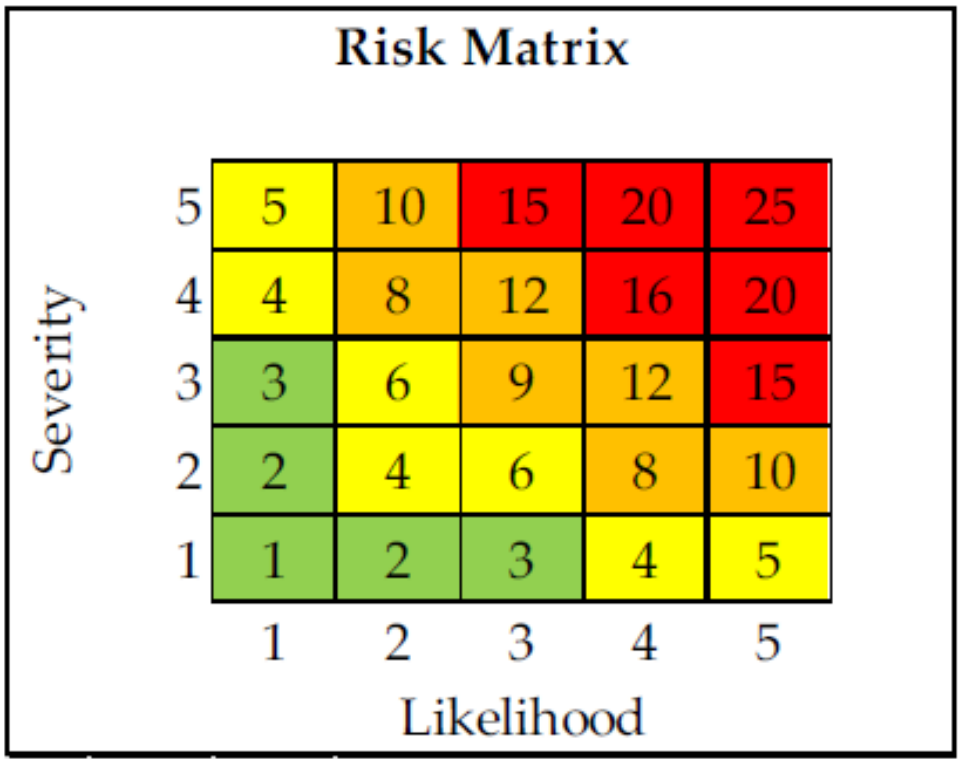

Figure 40: Risk matrix used for risk evaluation

Mitigation solutions are shown in Table 6.

Risk No.	Mitigation mesurement	Likelihood [1-5]	Severity [1-5]	Classification [1-25]
1.1	Do not wear loose clothing and tie hair	1	4	4
1.2	Use bolts to secure stainless steel container and autoclave to the vibrating table	1	3	3
3.1	Always make sure parts are secured.	1	3	3
3.2	Always turn off the amplifier when handling the ultrasonic transducer	1	3	3
3.3	To prevent a burst scenario, the autoclave was fitted with a safety valve actuating at 97 bar	1	2	2
3.5	To prevent a burst scenario, the autoclave was fitted with a safety valve actuating at 97 bar	1	2	2
4.1	Always make sure parts are secured.	1	3	3
5.1	Ensure ventilation when relieving the carbon dioxide.	1	5	5
5.2	Always make sure parts are secured.	1	3	3
5.2	Always make sure parts are secured.	1	3	3
5.3	Do not wear loose clothing and tie hair	1	3	3

Table 6: Risks that require mitigation and the corresponding mitigation

The location of the whole system is important because the ventilation needs to be sufficient. This is important in order to avoid the maximum allowed concentration of carbon dioxide. Figure 41 shows the scheme of the Department Petroleum Engineering (DPE) laboratory in Montanuniversität Leoben, Austria. The black dot represents the location where the system is going to be set.

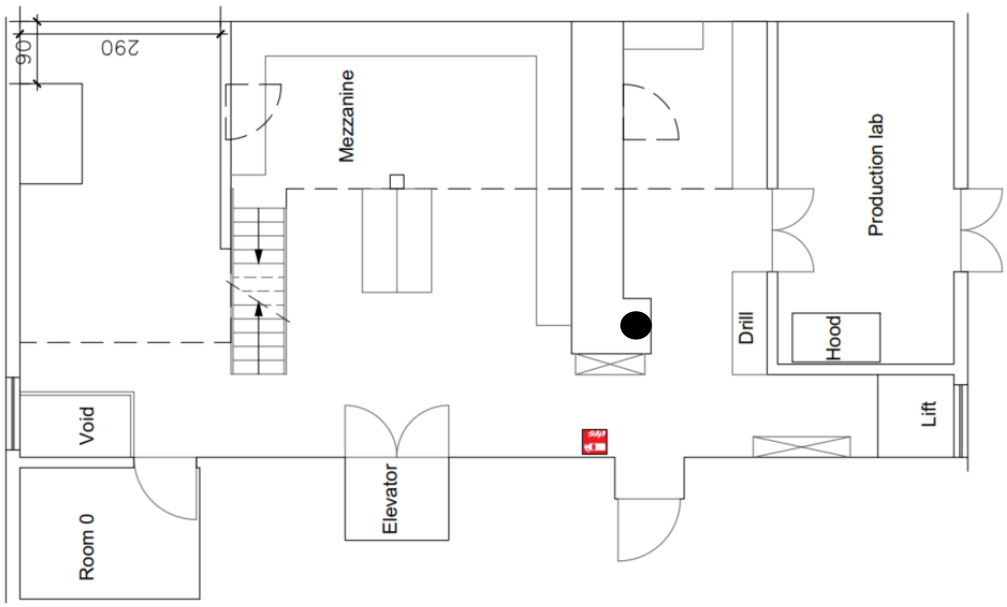

Figure 41: Scheme of the DPE lab with the marked position of the experimental system

When performing this experiment, theoretically there is a danger of gas leakage during the filling process and during the experiment. In order to identify this hazard and to warn personnel the ALTAIR 5X IR multi gas detector is employed, which is designed to perform a hazard assessment to:

- Assess potential worker exposure to combustible and toxic gases and vapors as well as low level of oxygen.
- Determine the appropriate gas and vapor monitoring needed for a workplace.

The ALTAIR 5X may detect combustible gases and certain combustible vapors. Also, it may be equipped to detect specific toxic gases for which a sensor is installed. Five sensors may measure 6 gases. It is also equipped with multiple alarms. This is made to increase user safety.

In case of gas leakage during the filling process, main valve of the cylinder needs to be closed, wait for 30 seconds, and observe gas detector value. If the detected level is not decreased, removed gas cylinder from the building to the open air and immediately contact with the gas supplier. If detected level is decreased, check all the connection in the experimental set up for the possible source of leaking using leakage spray. Fix it and repeat the filling process. During the experiment, cell needs to be transferred to the ventilation cabinet and slowly relieve pressure. Figure 42 shows the gas detector.

Figure 42: ALTAIR 5X IR multi gas detector

Chapter 5 Results and Discussion

This chapter presents the progress which was so far made for the project. Not all necessary things could have been done on time to present it in this thesis, but what would come up in the future will be also briefly explained in this chapter. As mentioned before, the acoustic system proved to be efficient to measure the compressive strength of the cement during carbonation. It is also important to note that correlations found in the literature may not be applied in general due to various parameters which influence the sonic velocity and compressive strength measurement. There, it is best to make measurements and make the correlation on your own. The results of that are going to be presented in this chapter.

First thing which needed to be done was to determine the cement composition for the experiments. There are two baseline experiments which are planned to do, namely the heavy carbonation baseline and the light carbonation baseline. The heavy carbonation baseline experiment indicates that the cement needs to have light density. This also means that the compressive strength of the cement is low. This means that the carbonation process will be intense for this type of cement. The light carbonation baseline experiment indicates that the cement needs to have heavy density. For that kind of cement, the compressive strength would be high, which means that the carbon dioxide would not cause that intensive carbonation compared to the light density cement.

The standard API test which determined the cement composition which is going to be used for the experiments is the free fluid test. According to the API RP 10B standard, the mixed and conditioned cement is put in the Erlenmeyer flask and there the cement is left to develop free fluid over the course of 2 hours. Goal for this test is to make the cement composition which is going to have the least amount of free fluid possible. In ideal case, there will not be any free fluid over the course of these 2 hours. Table 7 shows the free fluid results for the cement slurries. Under the Recommendation column the selected fluid composition may be read. The slurries which were prepared for this test had a volume of 600 cm^3.

Sample number with additives	Density (ppg)	Result (%)	Note	Recommendation
1 (15% BWOC)	12.3	4	Very viscous fluid	Reduce bentonite
2 (no additive)	17.2	1.33	Very viscous fluid	Add weight adder
3 (5% BWOC)	16	No result	Not pumpable	No bentonite for high density
4 (30% barite)	18	0.16	Visual estimation	Light carbonation baseline
5 (2,5% BWOC)	12.2	8	Prehydrated bentonite (30 min)	
6 (2,5% BWOC)	12.5	8	Prehydrated bentonite (night)	
7 (2,5% BWOC)	12.3	8	Prehydrated bentonite (2h)	30 min prehydration is sufficient
8 (5% BWOC)	12.4	2.16	Prehydrated bentonite (30 min)	Add more bentonite
9 (5,5 % BWOC)	12.5	1.67	Prehydrated bentonite (30 min)	Heavy carbonation baseline

Table 7: Free fluid results to determine slurry compositions for experiments

The primary unit for density used here is pounds per gallon. During the experiments, it was realized that prehydration would work better for light cement slurries. The prehydration means that the bentonite is mixed with water, then after some time under stationary conditions, the mixture is set to mix with cement to have increased viscosity and less free fluid compared to the ordinary mixture with bentonite. The time which is sufficient for prehydration process is found to be 30 minutes. Goal was to find the composition which has light density and the least amount of free fluid possible. During the tests, 0% of free fluid was not reached because for such a light cement slurry the mixture which could eventually have 0% free fluid would not be pumpable at all. Density of this slurry is 1.5 g/cm^3 (12.5 ppg).

The selected composition for 600 cm^3 of slurry for the heavy carbonation baseline is:

- 417 g cement,
- 460.5 g water and,
- 22.9 g bentonite.

For the light carbonation baseline experiment, the number of free fluid required to find the right composition was much. In this case, the goal of reaching 0% free fluid was much easier to achieve. The greatest constraint which needed to be met was that the water to

cement ratio should not be less than 0.4. This was achieved with the addition of barite, which functions as a weight adder. Density of this slurry is 2.16 g/cm^3 (18 ppg).

The selected composition for 600 cm^3 of slurry for the light carbonation baseline is:

- 761.1 g cement,
- 307.1 g water and,
- 304.4 g barite.

The next important thing which had to be done was the pressure test of the autoclave. As the autoclave has to be gas-tight, it should not allow any leaks. This means that there should not be any drop of pressure inside the autoclave. The autoclave is tightened with the bolts under a torque of 250 Nm. Figure 43 shows the setup for the pressure test.

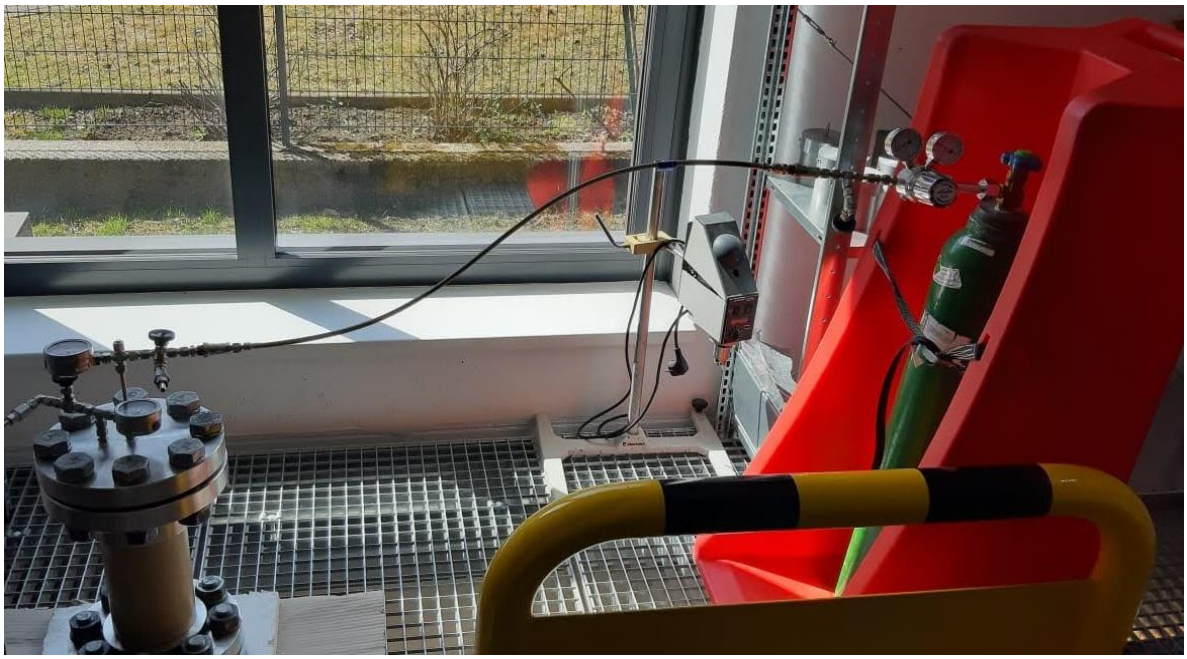

Figure 43: Pressure test setup

In this setup, the gas cylinder is connected to the autoclave with the pressure regulator, connector, and the gas line. Initial test was performed with argon, which is a noble gas. In this test, the pressure drop was not acceptable. No obvious leak could not have been found during the test. The leak check spray was used wherever there was a possible leak spot, but no bubbles were formed. Another pressure test was conducted with the carbon dioxide. The data for that pressure test are shown in Table 8 and Figure 44.

Date and time	Pressure (bar)	Notes
12.4.2021, 11:45	36	CO_2 bottle delivered, under influence of ambient temperature
13.4.2021, 09:00	46	Influence of ambient temperature removed
13.4.2021, 10:30	45	Pressure drop rate: 0.67 bar/h
13.4.2021, 11:50	43	Pressure drop rate: 1.5 bar/h
13.4.2021, 14:10	41	Pressure drop rate: 0.85 bar/h
14.4.2021, 09:45	35	Pressure drop rate: 0.31 bar/h
14.4.2021, 10:50	34	Pressure drop rate: 0.93 bar/h
14.4.2021, 12:45	32	Pressure drop rate: 1.04 bar/h
15.4.2021, 09:30	29	Pressure drop rate: 0.15 bar/h
15.4.2021, 11:25	28	Pressure drop rate: 0.52 bar/h
16.4.2021, 09:30	24	Pressure drop rate: 0.18 bar/h
16.4.2021, 14:35	22	Pressure drop rate: 0.39 bar/h
19.4.2021, 07:30	20	Pressure released

Table 8: Free fluid results to determine slurry compositions for experiments

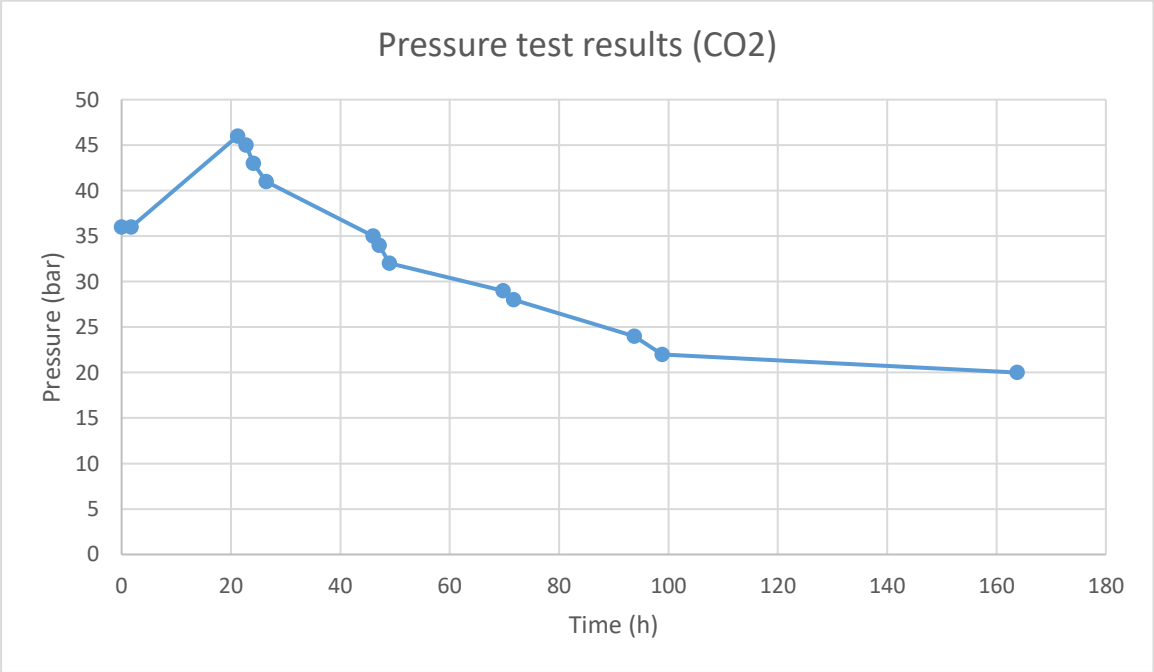

Figure 44: Graphical presentation of CO_2 pressure test results

Initially, with the influence of ambient temperature, which was colder at that time than the room temperature, the gas bottle could not deliver the maximum pressure. Therefore, the pressure test started with 36 bar and then increased to 46 bar once the influence of ambient temperature was completely removed. The results show that the majority of the maximum injected pressure dropped over the course of the test period. For this reason, the torque with which the bolts were tightened to flanges got increased from 250 to 300 Nm. The pressure test was done once again with an injection pressure of 50 bar. In this case, the pressure drop decreased. For 24 hours, the pressure dropped by only 2 bar, which was considered acceptable. To verify that there was no leak, additional pressure test of the autoclave in the water bath was performed, where no leak was detected.

To establish a correlation between the sonic velocity and the compressive strength of the cement, the uniaxial compressive strength test and acoustic measurements for both slurries were performed. Load cell was used to perform the uniaxial compressive strength test. The samples which were used for this test were the cylindric molds of cement slurries with the diameter of 28 mm and the length of 56 mm. In case that during the sample preparation the length is not exactly twice to diameter, correction for the uniaxial compressive strength was applied to get the correct compressive strength value. Sample surface has to be smooth and straight. This gives the best value of the compressive strength. The test was carried out over a period of 15 days. For each cement composition, 3 samples were used for a specific age. For this reason, the average value of the compressive strength is taken as the reference. Table 9 and Figure 45 show the uniaxial compressive strength related to the age of cement slurry for both slurries.

Age (days)	Average UCS of 12.5 ppg cement (MPa)	Average UCS of 18 ppg cement (MPa)
1	0.71	8.65
3	1.87	15.25
7	2.13	17.76
15	2.15	17.83

Table 9: UCS test results

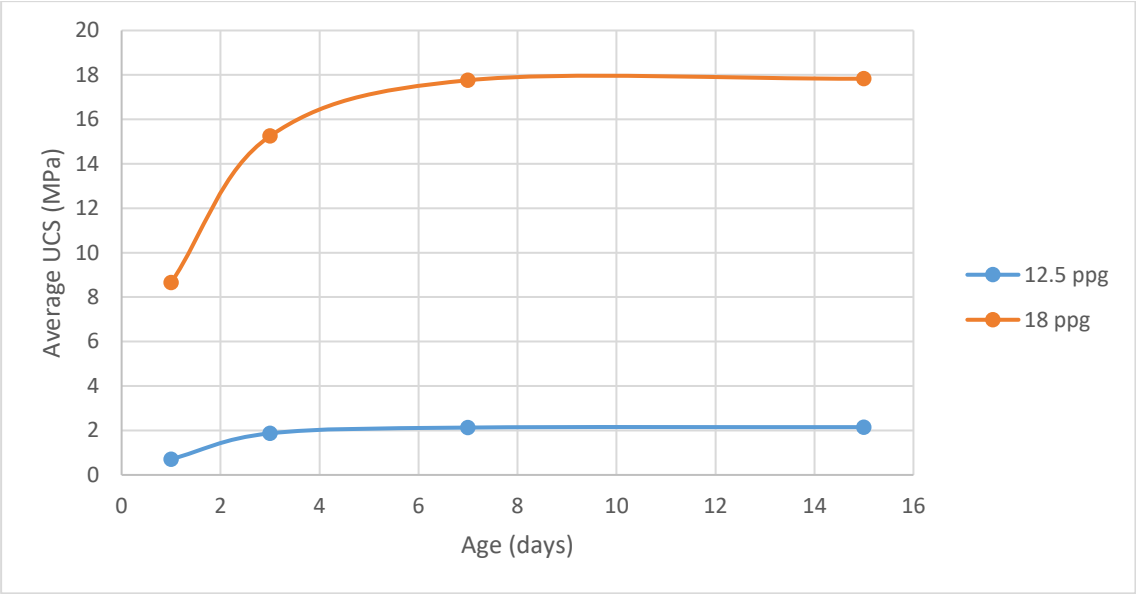

Figure 45: Graphical presentation of UCS test results

As it can be seen by the given results, the majority of compressive strength development takes place in the first week. After that, the compressive strength has a small increase over time. Also, the density and the water to cement ratio affect in a great way to the compressive strength. The light cement has a water to cement ratio of 1.1. The heavy cement has a water to cement ratio of 0.4.

To measure the sonic velocity, the acoustic equipment was used. To make sure the piezoelectric elements are tightly bonded to the sample, the clamps were used to put axial pressure on the elements. The greater axial pressure, the better reading would be of the sonic waves. As mentioned before, the first peak which was visible in the receiving wave was used as a reference for the arrival of the ultrasonic wave. There were 3 samples used for each type of cement, so the average results of sonic velocities were calculated. Table 10 present the results for sonic velocity.

Age (days)	Average sonic velocity of 12.5 ppg cement (m/s)	Average sonic velocity of 18 ppg cement (m/s)
1	804.7	1632
3	1083	1806
7	1237	2209
15	1298	2488

Table 10: Sonic velocity test results

The sonic velocity for 18 ppg slurry is much greater in comparison to the 12.5 ppg composition. This may be because of much higher density, which means in this context more cement particles that can be bonded together, thus greater sonic velocity comes out. For this reason, it may be concluded that the density affects both the compressive

strength and sonic velocity by increasing the values with the increased density. Figure 46 shows graphically the results of the sonic velocity measurements.

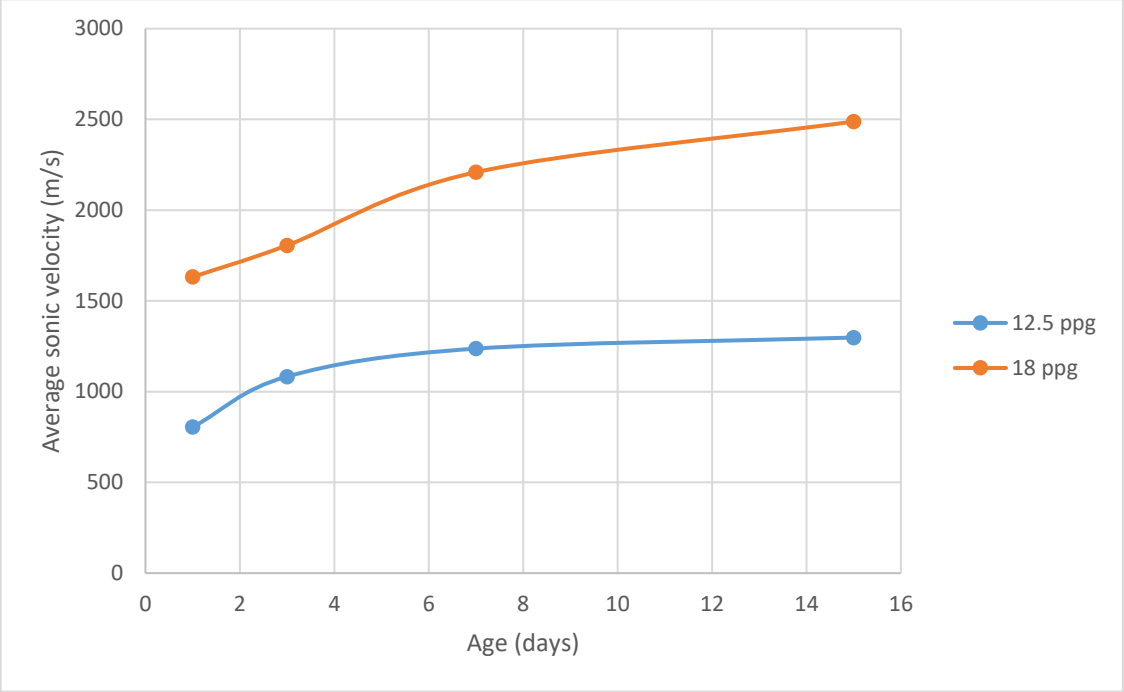

Figure 46: Graphical presentation of sonic velocity results

For the final step, the correlation between the compressive strength and the sonic velocity needs to be established. In this case, there will be two separate correlations due to two different densities and compositions of the cement slurry. Figure 47 shows the correlation for the 12.5 ppg slurry.

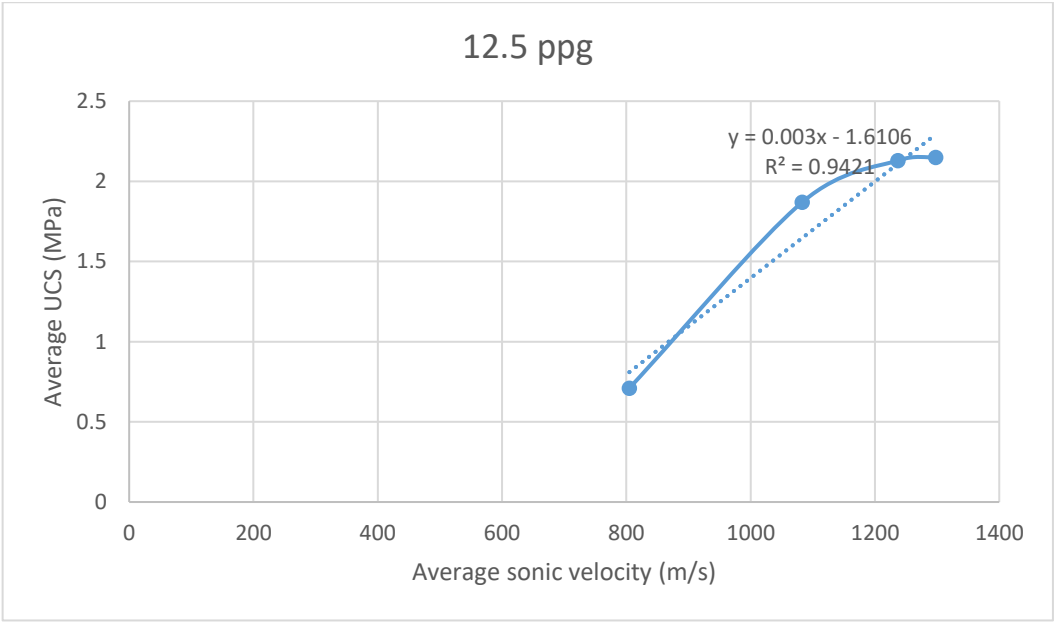

Figure 47: Correlation between sonic velocity and UCS for 12.5 ppg slurry

Based on the trend line, linear correlation between the sonic velocity and the uniaxial compressive strength is acceptable. Caution needs to be taken for the data points which were taken in the later stage of the measurement. As the compressive strength stops

developing that fast, there could be a different relationship between those two parameters in the later stages of cement development. There may also be some errors in compressive strength measurement, as not all samples could have been perfectly prepared for the test. In general, the linear relationship is considered to be acceptable to correlate the sonic velocity and the compressive strength of the cement. For the heavy cement slurry, Figure 48 shows the correlation between the sonic velocity and the uniaxial compressive strength.

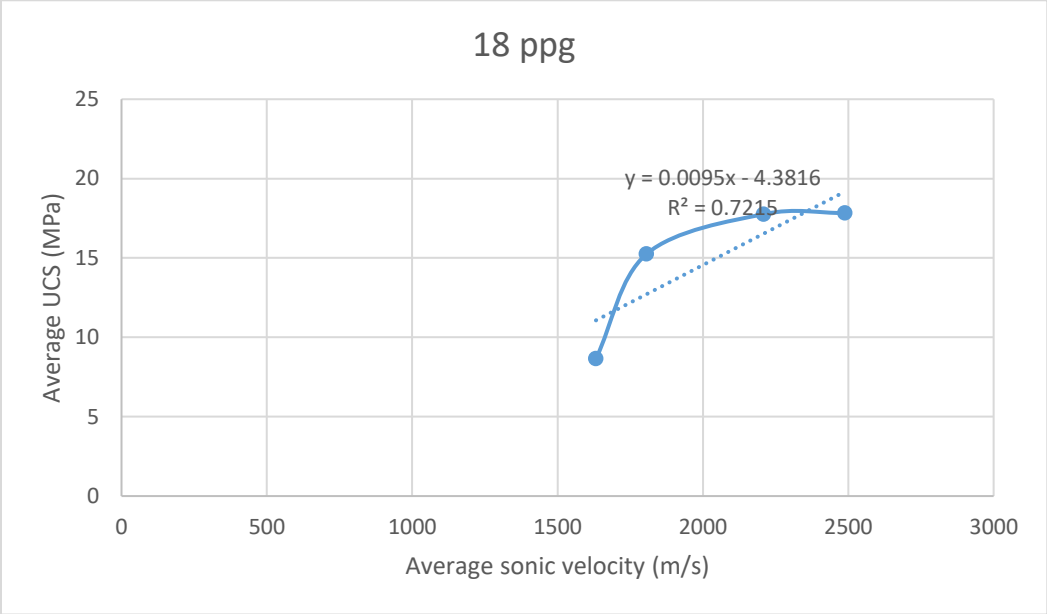

Figure 48: Correlation between sonic velocity and UCS for 18 ppg slurry

In this case, the linear trend line is not applicable to use for the correlation. The main reason for it could be that the sample preparation for the uniaxial compressive strength test was not easy at all. Some samples got broken when they got out of the cylindrical mold and also not all the samples had a straight surface after the preparation with the sandpaper. For this reason, the compressive strength measurements could be underestimated and therefore the correlation is not as good as in the previous composition and the example given earlier in this thesis.

The final part of the process which was done was the crack investigation. The purpose of this is to find out how the cracks alter the sonic velocity. Cracks also reduce the compressive strength of the cement so it can be assumed that there is also a correlation between cracks and sonic velocity. The bigger the crack, the slower the ultrasonic wave will pass through the cement.

For this purpose, 15 samples of the cement with same composition were made. The composition which was used to make the samples are the same ones applied so far (12.5 ppg, 5.5% prehydrated BWOC, 18 ppg, 30% barite). In total, there were 30 samples created for crack investigation.

The properties of a set of 15 samples is the following:

- 3 samples had a notch with the intended surface crack depth of 5 mm (5S),
- 3 samples had a notch with the intended surface crack depth of 10 mm (10S),
- 3 samples had a steel wire which formed an internal crack within the sample at the depth of 5 mm (5I),
- 3 samples had a steel wire which formed an internal crack within the sample at the depth of 10 mm (10I),
- 3 control samples which didn't have any defect (C)

The samples which were prepared were the cubic molds with the dimensions of 50.8x50.8 mm (2"x2"). These molds were selected because it was easier to cast the defects with them compared to the cylindrical samples, where multiple samples were prepared in one pipe. The pipe was cut to make the samples with proper dimensions after the cement was set. The notch was made from a steel sheet which was cut to the necessary dimensions to fit the cubic molds (5x5 cm), greased at the part where it was sunk into the cement. After greasing, it got to the targeted depth of the sample and glued on the edge of the mold. For the internal cracks, the steel wire was bent so that the majority of the wire would be positioned horizontally in the sample, greased at the part which will be in the cement, dived to the targeted depth and glued to the edge of the mold. After the cement was set, both the steel plates and the steel wires got pulled out of the cement so that cracks caused by them are left within the sample. Shallow depths were selected as greater crack depths would cause too much stress pulling the wire and the plates out. That amount of stress would cause the samples to be destroyed. After the wires and the plates got pulled out, the measurement process started. Sonic velocities were measured for the samples after 3,7, and 14 days after the samples got set. First measurement method which is going to be shown is the surface probing, where the transducers are set on the same surface on the sample. For this measurement, both transducers are set on an equal distance from the crack away (1.5 cm from each side). For the internal cracks, the same distance was applied from the spot where the hole was visible. Table 11 and Figure 49 show the surface probing results of the measurements for 12.5 ppg slurry.

Sample group/Age	3 days	7 days	14 days
5S	1087	1651	1839
10S	990	1415	1759
5I	1183	1734	1963
10I	1178	1632	1983
C	1230	1870	2031

Table 11: Average sonic velocities for 12.5 ppg slurry samples (in m/s, surface probing)

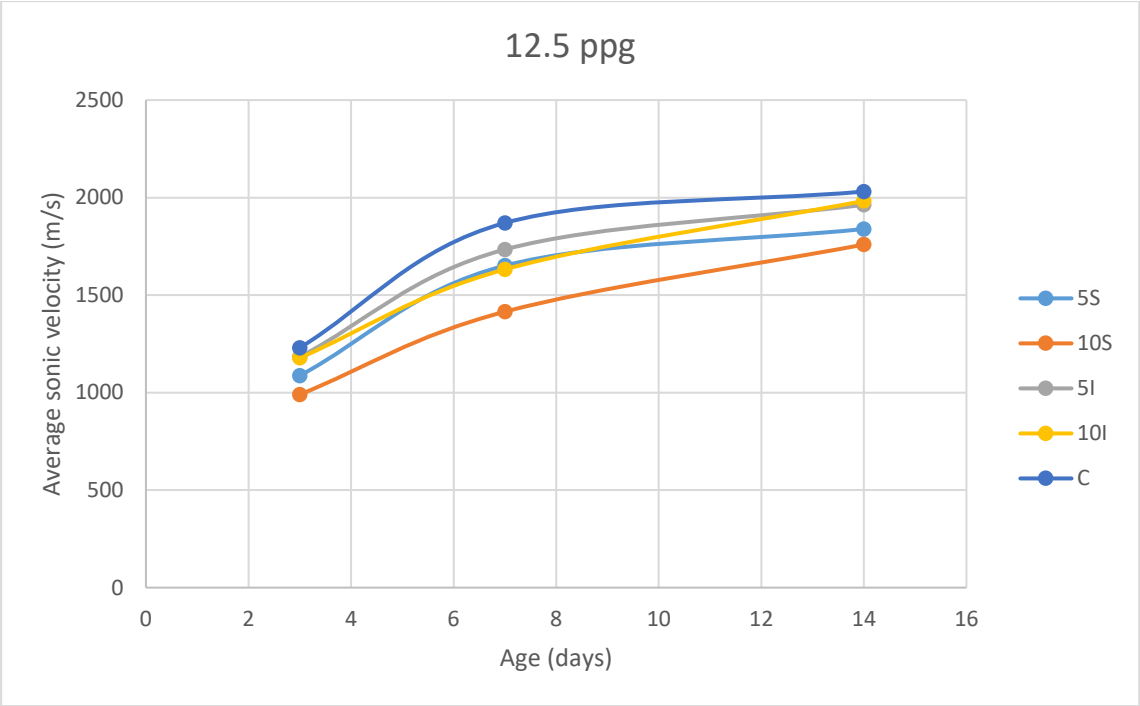

Figure 49: Graphical presentation of sonic velocity measurements for 12.5 ppg slurry (surface probing)

In this example, it can be seen that the surface cracks affect the sonic velocity the greatest when it comes to surface probing. Sonic velocity traveled the slowest through the 10S samples. The internal cracks also have an impact, but much less compared to the surface cracks. Table 12 and Figure 50 show the surface probing measurement results for the 18 ppg slurry.

Sample group/Age	3 days	7 days	14 days
5S	2407	2469	2568
10S	1924	2134	2188
5I	2633	2689	2765
10I	2580	2614	2642
C	2679	2701	2781

Table 12: Average sonic velocities for 18 ppg slurry samples (in m/s)

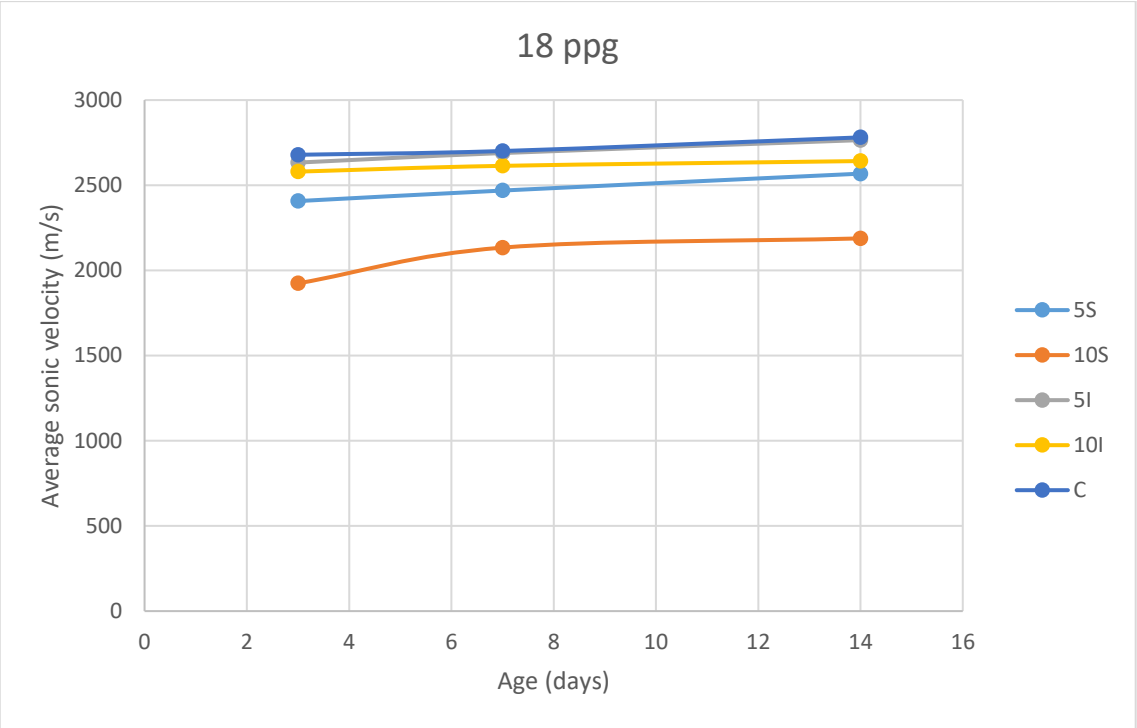

Figure 50: Graphical presentation of sonic velocity measurements for 18 ppg slurry

Seeing these results, the same conclusions can be made as in the previous group of samples for surface probing. In this case, the sonic velocity for the 10S samples is much slower compared to control samples as it stands out in Figure 50.

In addition to the sonic velocity measurements, the results were used to calculate the crack depth in mm. The actual crack depth for 5S samples was 5 millimeters and for 10S samples the actual crack depth was 10 millimeters. Equation 19 was applied to calculate the crack depth and results are shown in Table 13.

Sample group (density)	3 days	7 days	14 days	Average relative error (%)
5S (12.5 ppg)	7.95	7.97	7.02	52.93
10S (12.5 ppg)	11.05	12.96	10.55	15.2
5S (18 ppg)	7.33	6.67	6.25	35
10S (18 ppg)	14.54	11.65	11.78	26.57

Table 13: Calculated crack depth in mm for sample groups in surface probing

As presented in the previous table, calculated crack depth are overestimated compared to the actual crack depth. The least error was found in the 10S samples for the 12.5 ppg density, while the greatest error was found for the 5S samples for the same density.

Another potential indicator of cracked samples found during the measurement process is the peak-to-peak voltage the samples can give. The greatest peak-to-peak voltage on the receiving piezoelement got recorded along with the sonic velocity measurement. The reason for this was that the surface waves release the greatest amount of energy, so the waves from it can be the easiest to record and measure. Table 14 shows the average

maximum peak-to-peak voltage for 12.5 ppg slurry, while Table 15 shows the average maximum peak-to-peak voltage for 18 ppg slurry.

Sample group/Age	3 days	7 days	14 days
5S	20	45.4	58
10S	13.33	47.5	58.5
5I	48.33	59.2	40.31
10I	40	63.2	101
C	25	155	123

Table 14: Average maximum peak-to-peak voltage for 12.5 ppg slurry samples (in mV) (surface probing)

Sample group/Age	3 days	7 days	14 days
5S	50	73.2	62
10S	88.3	98.3	103
5I	92.5	85	156
10I	80	57.5	102
C	250	131	171

Table 15: Average maximum voltage for 18 ppg slurry samples (in mV) (surface probing)

By the previous results shown in Table 14 and 15, it can be concluded that the maximum peak-to-peak voltage can be only as a rough indicator that a crack is present. The results are hard to correlate, as there is no pattern present on how much does the maximum peak-to-peak voltage increase. In some cases, this also decreases. In general, the greatest maximum peak-to-peak voltage is present in the control samples (no cracks present) and the maximum peak-to-peak voltage is reduced in the cracked samples compared to the control samples. For the control sample for the 12.5 ppg slurry this was not the case, but this can be treated as an exception to the rule.

The second measurement method which was applied for crack investigation was the direct probing. In this case, the piezoelements were set on the opposite sides of the samples and in a way that the ultrasonic wave had to pass through the crack to get to the receiving piezoelement. This means that the piezoelements were set on the top part of the samples, where the cracks were located. Table 16 and Figure 51 show the results of the measurement for the 12.5 ppg slurry.

Sample group/Age	3 days	7 days	14 days
5S	1061	1424	1442
10S	1018	1360	1373
5I	1173	1361	1366
10I	1173	1450	1455
C	1176	1464	1464

Table 16: Average sonic velocities for 12.5 ppg slurry samples (in m/s) (direct probing)

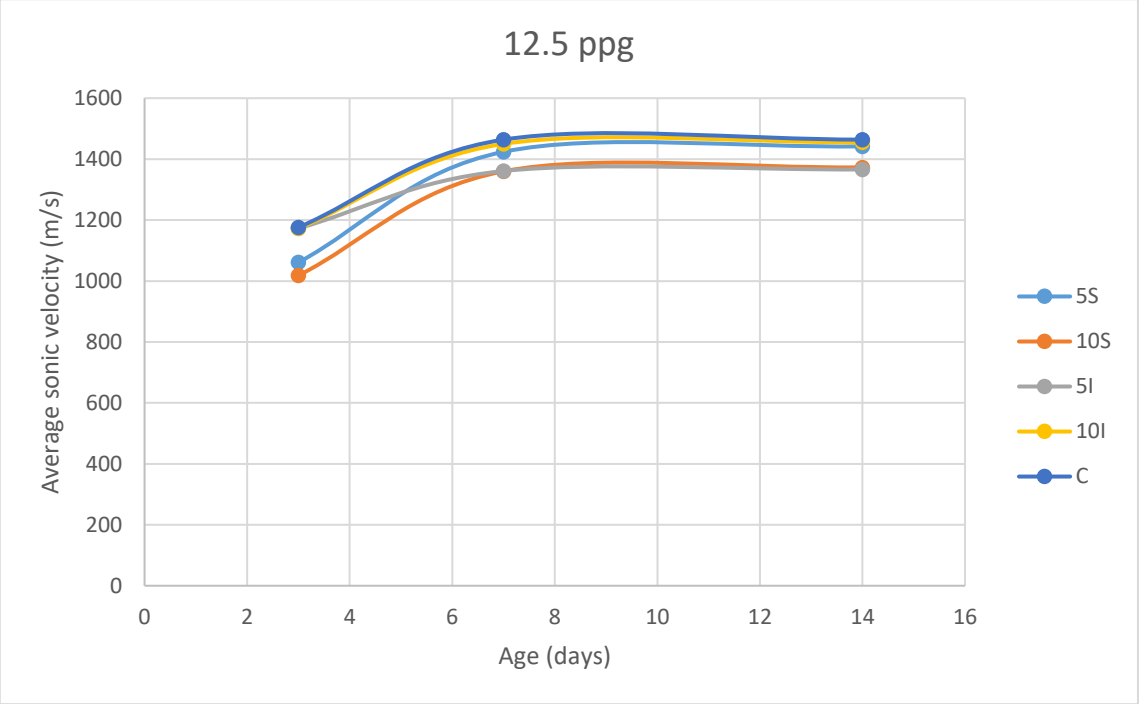

Figure 51: Graphical presentation of sonic velocity measurements for 12.5 ppg slurry

As it was present in the surface probing, the same pattern is visible in direct probing. The slowest sonic velocity appears to be in the 10S samples and samples with the surface crack retard the ultrasonic waves greater compared to the samples with internal cracks. Compared to the surface probing, the velocities in direct probing are in general slower. Table 17 and Figure 52 show the measurement results for direct probing for 18 ppg slurries.

Sample group/Age	3 days	7 days	14 days
5S	2314	2366	2369
10S	2260	2354	2355
5I	2452	2529	2538
10I	2389	2454	2460
C	2489	2564	2618

Table 17: Average sonic velocities for 18 ppg slurry samples (in m/s) (direct probing)

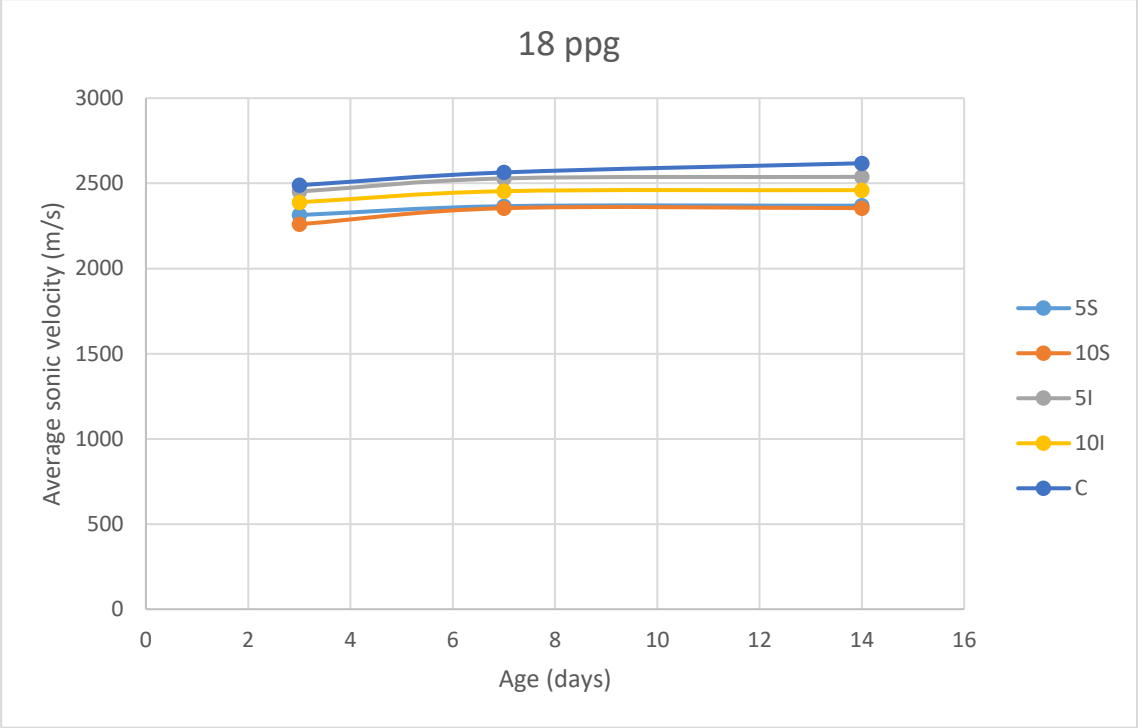

Figure 52: Graphical presentation of sonic velocity measurements for 18 ppg slurry

The pattern which was present in the 12 ppg slurry is also present for 18 ppg slurry samples. In this case, the velocity is also slower in direct probing compared to the surface probing, but the difference in velocities is less for 18 ppg samples. Surface cracks alter the sonic velocity the greatest, where the slowest sonic velocities are present again in 10S samples. The peak-to-peak voltage measurements also were made for direct probing. Table 18 and Table 19 show the results for the average maximum peak-to-peak voltage for 12.5 ppg and 18 ppg, respectively.

Sample group/Age	3 days	7 days	14 days
5S	41.7	160	343
10S	55	144	126
5I	273	376	432
10I	138	244	337
C	210	593	562

Table 18: Average maximum peak-to-peak voltage for 12.5 ppg slurry samples (in mV) (direct probing)

Sample group/Age	3 days	7 days	14 days
5S	167	169	110
10S	142	90.5	73.6
5I	163	272	235
10I	81.7	97.3	91.5
C	260	299	271

Table 19: Average maximum peak-to-peak voltage for 18 ppg slurry samples (in mV) (direct probing)

By the previous results shown in Table 18 and Table 19, the same conclusions can be made as it was in the surface probing. The peak-to-peak voltage may only be an indicator of damaged cement as it is again hard to correlate the results of the measurements. In general, again, the greatest maximum peak-to-peak voltage is present in the control samples (no cracks present) and the maximum peak-to-peak voltage is reduced in the cracked samples compared to the control samples. For the control sample for the 12.5 ppg slurry this was again not the case, but this can be treated as an exception to the rule.

The third and final measurement type used for crack investigation is the so called 'deep direct' probing. This is not officially classified in the literature, but the goal here is to actually find the sonic velocities in the part of the samples which is not affected by cracks. As the piezoelements are located at the bottom part of the samples in this case, that's how deep direct probing got its name. Table 20 and Figure 53 show the measurement results for this type of probing for 12.5 ppg slurry.

Sample group/Age	3 days	7 days	14 days
5S	1162	1437	1448
10S	1095	1420	1437
5I	1158	1357	1388
10I	1162	1367	1451
C	1176	1464	1464

Table 20: Average sonic velocities for 12.5 ppg slurry samples (in m/s) (deep direct probing)

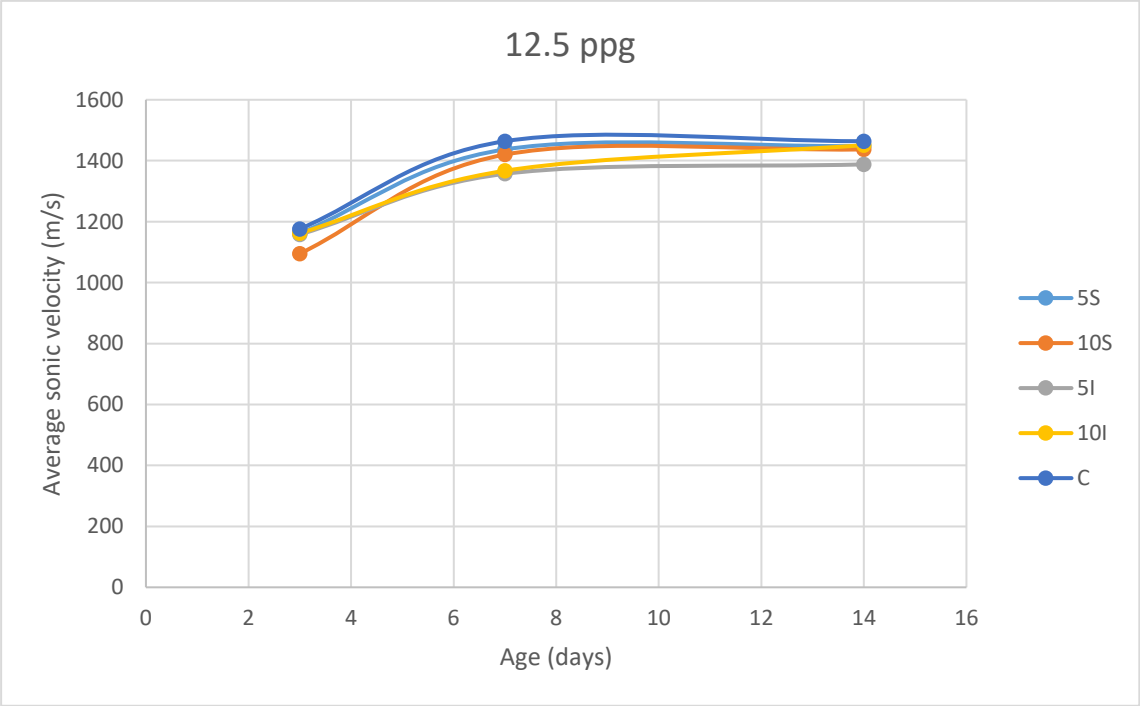

Figure 53: Graphical presentation of sonic velocity measurements for 12.5 ppg slurry

Sonic velocity for the cracked samples is slower, but there is a small difference compared to normal direct probing. In one case, the sonic velocities in the internal crack is slower compared to the samples with the surface cracks. This would mean that when deep direct probing is applied, a.k.a. probing in slurries anywhere where cracks are present, this can only be used as an indicator of cracks present. For the location of cracks to be found, there needs to be a greater different of sonic velocities between damaged and clean cement slurries. This can be also seen for the 18 ppg slurries. Table 21 and Figure 54 show the results of deep direct probing for that kind of slurry samples.

Sample group/Age	3 days	7 days	14 days

5S	2285	2375	2399
10S	2332	2409	2444
5I	2305	2390	2421
10I	2301	2397	2428
C	2489	2564	2618

Table 21: Average sonic velocities for 18 ppg slurry samples (in m/s) (deep direct probing)

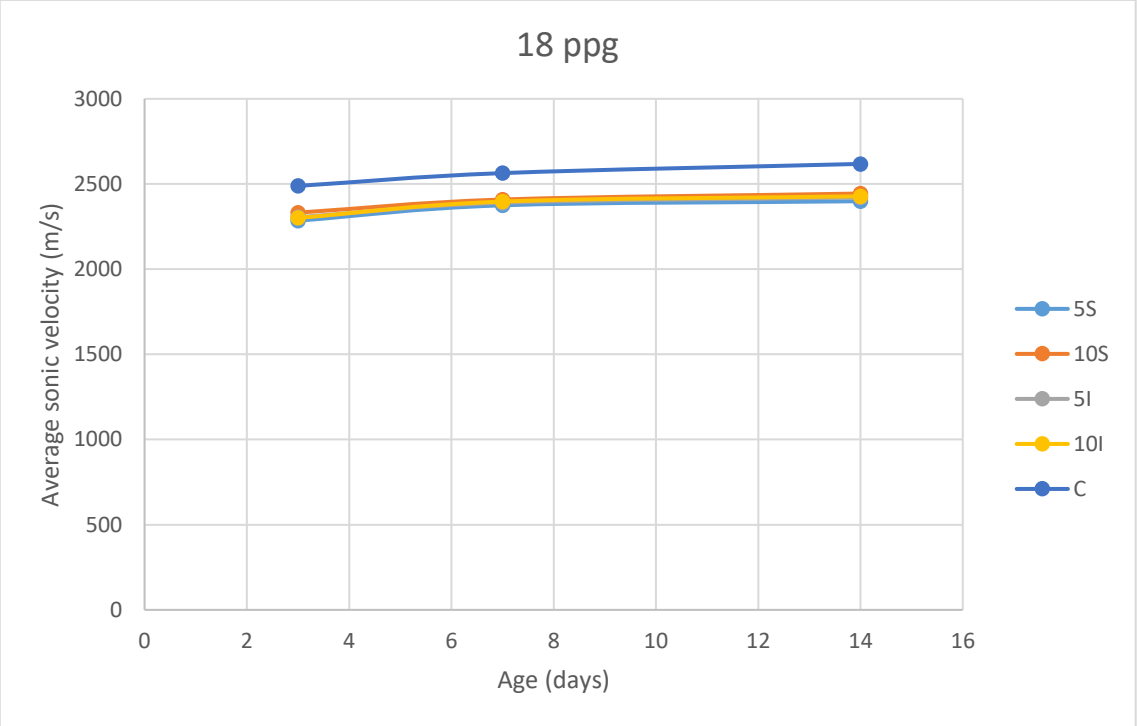

Figure 54: Graphical presentation of sonic velocity measurements for 18 ppg slurry

As mentioned before, the deep direct probing can be used as an indicator that the damage is somewhere present. This is showcased best at this example. The sonic velocities of the damaged samples are graphically close together and have a very small difference between each other. However, they all have some difference in sonic velocities compared to the control samples, which can also be graphically visible as the sonic velocities from clean and damages samples are separated. The maximum peak-to-peak voltage measurements were also taken for this kind of probing. Table 22 and Table 23 show the average maximum peak-to-peak voltage for 12.5 ppg and 18 ppg slurry samples respectively.

Sample group/Age	3 days	7 days	14 days

5S	115	461	553
10S	193	225	464
5I	255	410	676
10I	185	539	457
C	210	593	562

Table 22: Average maximum peak-to-peak voltage for 12.5 ppg slurry samples (in mV) (deep direct probing)

Sample group/Age	3 days	7 days	14 days
5S	250	222	173
10S	227	178	152
5I	183	327	485
10I	223	325	208
C	260	299	271

Table 23: Average maximum peak-to-peak voltage for 18 ppg slurry samples (in mV) (deep direct probing)

The rule works the same way as in the other probing types. In general, the control samples have the greatest maximum peak-to-peak voltages, and the cracked samples have it reduced compared to the clean samples. Of course, exceptions to the rule are also present, even more in this case. Therefore, the peak-to-peak can be always applied as a potential indicator of damage. Finally, all the samples which were used for crack investigation got destroyed in the load cell to see how much do the crack affect the compressive strength of the cement. Results of the average UCS for 12.5 ppg and 18 ppg slurry are shown in Table 24.

Sample group	Average UCS for 12.5 ppg slurry (MPa)	Average UCS for 18 ppg slurry (MPa)
5S	4.27	33.8
10S	3.31	33.8
5I	4.21	40.4
10I	5.32	40.7
C	5.53	44.6

Table 24: Average UCS after 14 days for different sample groups

In general, it may be concluded that as it is the case for sonic velocities, the surface cracks affect the compressive strength greater compared to the internal cracks. Also, the greater the surface crack, the compressive strength of the cement is usually less.

What was so far done was the base for the future experimental process. Unfortunately, during the project, there were some setbacks. The setbacks occurred in the order and delivery time of some components. This happened because the current pandemic slowed everything down and made the delivery from abroad more complicated. For this reason, the whole experimental process could not have been done on time.

In the future, the pumping system should arrive soon, which would allow to perform the experimental process with the supercritical carbon dioxide. As the carbon dioxide cylinder has a maximum pressure of 57 bar with which the carbon dioxide may be injected, the pumping system would help to raise the pressure to at least 75 bar, which is enough for supercritical conditions. It may also show the volume of carbon dioxide which was injected into the autoclave.

The experiments should go according to the procedure mentioned earlier in this thesis. The goal is to ensure the current design is also applicable for two real-time monitoring methods of carbonation, namely the acoustic method and the computed tomography scan. The results of the real-time methods are going to be verified with multiple destructive tests.

Chapter 6 Conclusion

The thesis showed that the acoustic measurement is a suitable way to measure the compressive strength of the cement. This was shown with the previous works which were made with the ultrasonic pulse velocity method for concrete and the linear correlation of the sonic velocity with the compressive strength for the light slurry. The heavy slurry unfortunately did not show a good correlation of these two properties. For this composition, caution needs to be taken. The samples were not always prepared in the best way possible, as sample preparation is the hardest part for compressive strength measurement. Therefore, the compressive strength of some samples could have been underestimated, which contributed to the nonlinearity of the correlation. The equipment used to measure the acoustic signals proved to be applicable in real-time. It may measure the signals as long as the software runs on a computer. For the sample measurements, the waveforms which were shown on the receiving channel were consistent during the measurement process. This means the accuracy of the measuring system is good. Crack investigation showed that cracks alter the sonic velocity of the ultrasonic waves. The surface cracks showed to alter the sonic velocity greater compared to internal cracks. With the suggested formula, the crack depth may be calculated, but caution needs to take place as it usually leads to overestimation of the calculated crack depth compared to the actual crack depth. Another potential indicator of cracks could be the voltage at the receiving transducer as well. As the waves pass through the crack, energy is lost, therefore it can be also used to determine cracks in the cement. For a more precise and more comfortable process of using the acoustic measurements, a more extensive database is necessary. This database needs to include cement designs which were already used for these tests and also other cement designs various densities and compositions.

The current design of the autoclave was proven to be gas tight and ready for the experiment. As shown with the previous work, this autoclave should also be applicable for real-time monitoring of carbonation of the cement, which is the ultimate goal for this thesis. Some parts of the experimental process were not done on time to be mentioned in the thesis. These parts will be further investigated in the future. To know the exact amount of the carbon dioxide injected in the autoclave and to ensure the supercritical conditions for the carbon dioxide, a pumping system should be installed.

Finally, carbonation of cement could have an extreme influence on the cement and its integrity. Cement compositions have to be studied for the resistance of carbonation prior to their application.

Bibliography

1. Aiex, C., Campos, G., Deshpande, A. et al., 2015. An Experimental Study on Effects of Static CO2 on Cement under High-Pressure/High-Temperature Conditions. OTC 25659-MS

2. Air Liquide. Gas Encyclopedia, https://encyclopedia.airliquide.com/

3. Allinson, W.G., Nguyen, D.N., and Bradshaw, J. 2003. The Economics of Geological Storage of CO2 in Australia. The APPEA Journal 43 (1): 623. https://doi.org/10.1071/AJ02035

4. ANSI/API 10A/ISO 10426-1-2001, API Specification for Cements and Materials for Well Cementing. 2002. Washington D.C.: American Petroleum Institute

5. Anthony, J.W. 1995. Handbook of Mineralogy. Chantilly, VA, USA: Mineralogical Society of America

6. Baehaki et al. 2019. Experimental study of crack depth measurement of concrete with ultrasonic pulse velocity (UPV). IOP Conference Series: Materials Science and Engineering. Volume 674. Broad Exposure to Science and Technology 2019 (BEST 2019). Bali. Indonesia

7. Barret, P. 1986. Hydration Mechanism of Calcium Silicates (C3S, C2S), Cement Compounds, Through the General Concepts of the Reactivity of Solids.

8. Bock, B., Rhudy, R., Herzog, H. et al. 2003. Economic Evaluation of CO2 Storage and Sink Enhancement Options. https://doi.org/10.2172/826435

9. Brown, P.W., Franz, E., Frohnsdorff, G. et al. 1984. Analyses of the Aqueous Phase During Early C3S Hydration. Cement and Concrete Research 14 (2): 257-262. https://doi.org/10.1016/0008-8846(84)90112-1.

10. Bruckdorfer, R.A., 1986. Carbon Dioxide Corrosion in Oilwell Cements. In SPE Rocky Mountain Regional Meeting. Society of Petroleum Engineers. https://doi.org/10.2118/15176-MS.

11. Burrascano, P., Callegari, S., Montisci, A. et al. (eds.). 2015. Ultrasonic Nondestructive Evaluation Systems: Industrial application issues. Cham: Springer. https://doi.org/10.1007/978-3-319-10566-6.

12. Chandler Engineering Company. 2015. a. Instruction Manual Model 3260 Constant Speed Mixer

13. Chandler Engineering Company . 2015. b. Instruction Manual Model 1200 Atmospheric Consistometer

14. Chandler Engineering Company. 2015. c. Instruction Manual Model 8300 Pressurized Consistometer

15. Chandler Engineering Company. 2016. Instruction Manual Model 7120 Stirred Fluid Loss Cell

16. Chandler Engineering Company. 2018. Instruction Manual Model 4265-HT High Temperature UCA

17. Chegg. 2020. CO2 phase diagram, URL: https://www.chegg.com/homework-help/questions-and-answers/corresponding-co2-phase-diagram-schematically-draw-gibbs-energies-function-temperature-pha-q19601788

18. EPA. 2021. Greenhouse Gas (GHG) Emissions, URL: https://www.epa.gov/ghgemissions

19. Galbadini. 2021. Quasar 200 datasheet Quasar 200 - Material Testing machine (galdabini.eu)

20. Geoengineer. 2021. Splitting Tensile Strength Test (Brazilian) https://www.geoengineer.org/index.php/education/laboratory-testing/splitting-tensile-strength-test-brazilian

21. Glasser, D., Lachowski, L.S., Mohan, K. et al. 1978. A Multi-Method Study of C3S Hydration. Cement and Concrete Research 8 (6): 733-739. https://doi..org/10.1016/0008-8846(78)90082-0.

22. Goel, M., Sudhakar, M., and Shahi, R.V. 2018. Carbon Capture, Storage and Utilization: A possible climate change solution for energy industry. BocaRaton, FL: Routledge, Taylor, and Francis Group.

23. Hendricks, C., Crijns-Graus, W., Bergen, F. 2004. Global Carbon Dioxide Storage Potential and Costs. INIS 35 (26).

24. IEA. 2016. 20 Years of Carbon Capture and Storage-Accelerating Future Deployment, https://www.oecd.org/publications/20-years-of-carbon-capture-and-storage-9789264267800-en.htm

25. IPCC. 2014. Climate Change 2014 Mitigation of Climate Change, Cambridge University Press

26. Institute for 21st century. 2012. CO2 Enhanced Oil Recovery.

27. Jobard, E., Sterpenich, J., Pironon, J. et al., 2018. Experimental Modelling of the Caprock/Cement Interface Behavior under CO2 Storage Conditions: Effect of Water and Supercritical CO2 from a Cathodoluminescence Study. Geosciences 8 (5), p.185 https://doi.org/10.3390/geosciences8050185

28. Kalyan, T.S., Kishen, J.M.C. 2014. Experimental Evaluation of Crack in Concrete by Ultrasonic Pulse Velocity. Asia Pacific Conference on Non-Destructive Testing (14th APCNDT). Mumbai. India

29. Krautkrämer, J., Krautkrämer, H. 1990. Ultrasonic Testing of Materials, fourth Fully Revised Edition. Berlin, Heidelberg: Springer. https://doi.org/10.1007/978-3-662-10680-8.

30. Lacerda, E. Magalhaes, A.G., Bernardes, E.E. et al., 2017. Monitoring the carbonation front progress in a cementitious composite having its pore structure analyzed through micro-CT imaging. Rev. IBRACON Estrut. Mater. 10 (3): 653-668. https://doi.org/10.1590/s1983-41952017000300006.

31. Lee, Y.H., Oh, T. 2016. The Measurement of P-, S-, and R-Wave Velocities to Evaluate the Condition of Reinforced and Prestressed Concrete Slabs. Hindawi Publishing Corporation. http://dx.doi.org/10.1155/2016/1548215

32. Mathez, E.A., Smerdon, J.E., 2018. Climate change: The Science of Global Warming and our Energy Future, Second edition. New York: Columbia University Press

33. Metz, 2005. IPCC Special Report on Carbon Dioxide Capture and Storage. Cambridge: Cambridge University Press.

34. Naik, T.R., Malhotra, V.M., Popovics, J.S. 2004. Handbook on Nondestructive Testing of Concrete. CRC Press LLC

35. Nelson, E.B: and Guillot, D. 2006. Well Cementing, second ed. Sugar Land, Tex.: Schlumberger

36. Onan, D.D. 1984. Effects of Supercritical Carbon Dioxide on Well Cements. In Permian Basin Oil and Gas Recovery Conference. Society of Petreoleum Engineers. https://doi.org/10.2118/12593-MS.

37. Österreichische Bundesverfassung. 2004. Verordnung des Bundesministers für Wissenschaft, Forschung und Wirtschaft über sicherheitstechnische Bestimmungen für Prüfungen bei der Inbetriebnahme und während des Betriebes von Druckgeräten (Druckgeräteüberwachungsverordnung): DGÜW-V.

38. PI Ceramic GmbH. 2020. Fundamentals of Piezo Technology, https://www.piceramic.com/.

39. Pittino, G. 2020. Lecture notes from course 'Well Construction Mechanical Lab'. Chair of Subsurface Engineering, Montanuniversität Leoben

40. Prohaska, M. 2020. Lecture notes from course 'Well Construction Fluids Lab'. Chair of Drilling and Completion Engineering, Montanuniversität Leoben

41. Rupitsch, S.J. 2019. Piezoelectric Sensors and Actuators: Fundamentals and Applications. Berlin, Heidelberg: Springer Berlin Heidelberg. https://doi.org/10.1007/978-3-662-57534-5.

42. Saini, D. 2017. Engineering Aspects of Geologic CO2 Storage: Synergy between Enhanced Recovery and Storage. Cham, s.l.: Springer International Publishing. https://doi.org/10.1007/978-3-319-56074-8.

43. Seevam, P.N., Downie, M.J., and Race, J.M. 2007. Transport of CO2 for Carbon Capture and Storage in the UK. In SPE Offshore Europe Oil and Gas Conference and Exhibition. Society of Petroleum Engineers. https://doi.org/10.2118/109060-MS.

44. Schlumberger Oilfield Glossary. 2021. Uniaxial Compressive Strength https://glossary.oilfield.slb.com/en/terms/u/uniaxial_compressive_strength

45. Tumidajski, P.J. and Thomson, M.L. 1994. Influence of cadmium on the hydration of C3A. Cement and Concrete Research 24 (7): 1359-1372. https://doi.org/10.1016/0008-8846(94)90121-X.

46. Vicente, M.A., Minguez, J.M., Gonzalez D.C. 2017. The Use of Computed Tomography to Explore the Microstructure of Materials in Civil Engineering: From Rocks to Concrete. InTech http://dx.doi.org/10.5772/intechopen.69245

47. Wagner, P., 2020. Real-Time Monitoring of the Effect of Carbon Dioxide on the Cement Sheath, Master's Thesis, Montanuniversität Leoben, 2020

Acronyms

EPA	Environmental Protection Agency
IPCC	Intergovernmental Panel on Climate Change
CCS	Carbon Capture and Storage
IEA	International Energy Agency
EOR	Enhanced Oil Recovery
WAG	Water Alternating Gas
API	American Petroleum Institute
MSR	Moderate sulfate resistant
HSR	High sulfate resistant
WTI	West Texas Intermediate
CT	Computer Tomography
UCS	Uniaxial Compressive Strength
SEM	Scanning Electron Microscopy
XRD	X-ray diffraction
PZT	Lead zirconate titanate
UPV	Ultrasonic Pulse Velocity
PEEK	Polyether Ether Ketone
USB	Universal Serial Bus
ISRM	International Society for Rock Mechanics
DTS	Direct Tensile Strength
BTS	Brazilian Tensile Strength
RP	Recommended Practice
UCA	Ultrasonic Cement Analyzer
RPM	Revolutions per minute
EN	European Norm
PN	Pressure Nominal
DN	Diameter Nominal
NPT	National Pipe Thread
HT	High Temperature
PC	Personal Computer
DGÜW-V	Druckgeräteüberwachungsverordnung

Symbols

v_p	P-wave velocity	[m/s]
v_s	S-wave velocity	[m/s]
v_R	R-wave velocity	[m/s]
E_d	dynamic Young's modulus	[Pa]
v_d	dynamic Poisson's ratio	[-]
φ	density	[kg/m^3]
$\sin_{\alpha 1}$	sine of the angle between the reflected P-wave direction and the middle line	[-]
$\sin_{\alpha 2}$	sine of the angle between the transmitted P-wave direction and the middle line	[-]
$\sin_{\beta 1}$	sine of the angle between the reflected S-wave direction and the middle line	[-]
$\sin_{\beta 2}$	sine of the angle between the transmitted S-wave direction and the middle line	[-]
R	reflected fraction	[-]
Z	acoustic impedance	[kg/m^{2}s],
T	transmitted fraction	[-]
h	crack depth	[m]
x	distance between crack and the piezoelement	[m]
t	time	[s]
σ	compressive strength	[MPa]
σ_t	tensile strength	[MPa]
d	diameter	[mm]
l	length	[mm]
P	load	[N]
w	width	[mm]

List of Figures

List of Tables